Chemical Science

ROYAL SOCIETY OF CHEMISTRY

REVIEW

View Article Online
View Journal | View Issue

Cite this: *Chem. Sci.*, 2026, **17**, 5820

Advances in MgAgSb thermoelectrics: from materials to devices

Liangjun Xie,[a] Ran He, *[a] Jiehe Sui, [b] Kornelius Nielsch[a] and Zihang Liu *[c]

Thermoelectric materials have attracted considerable attention due to their significant potential in waste heat recovery and solid-state cooling, which are critical for emerging technologies such as the Internet of Things, 5G communications, and thermal management of advanced electronics. In the field of low-temperature thermoelectric materials and devices, MgAgSb-based devices have emerged as a promising alternative to commercial Bi_2Te_3-based devices, owing to their superior performance near room temperature, abundant elemental availability, and environmental compatibility. Over the past decade, substantial progress has been achieved in elucidating and optimizing the thermoelectric properties of MgAgSb and its devices. This review presents a comprehensive summary of recent developments in the intrinsic properties, synthesis process refinements, and performance optimization strategies of MgAgSb, as well as interface engineering, geometric optimization, and stability enhancement in MgAgSb-based devices, while critically addressing current challenges and prospective pathways toward the practical implementation of MgAgSb-based thermoelectrics.

Received 23rd September 2025
Accepted 15th February 2026

DOI: 10.1039/d5sc07399e

rsc.li/chemical-science

1 Introduction

Thermoelectric materials enable the direct conversion of thermal energy into electrical energy, offering significant potential for waste heat recovery and solid-state cooling applications.[1–5] In particular, low-temperature thermoelectric materials have attracted considerable attention for solid-state cooling, driven by advancements in electronic chips, the Internet of Things, and 5G technologies.[6–10] It is reported that the total waste-heat potential in the European Union is approximately 300 TWh per year, of which one-third corresponds to low-temperature waste heat below 200 °C and an additional 25% falls within the 200–500 °C range.[11] These findings clearly demonstrate the substantial potential for low-temperature waste-heat recovery using thermoelectric

[a]*Leibniz Institute for Solid State and Materials Research, 01069, Dresden, Germany. E-mail: r.he@ifw-dresden.de*

[b]*National Key Laboratory for Precision Hot Processing of Metals, Harbin Institute of Technology, Harbin 150001, China*

[c]*State Key Laboratory of Precision Welding & Joining of Materials and Structures, Harbin Institute of Technology, Harbin, 150001, China. E-mail: zihangliu@hit.edu.cn*

Liangjun Xie

Liangjun Xie is a postdoctoral researcher at the Leibniz Institute for Solid State and Materials Research (IFW Dresden), Germany, supported by the Alexander von Humboldt Fellowship since 2026. He received his PhD from the Harbin Institute of Technology in 2023. His research focuses on Mg-based thermoelectric materials for thermoelectric cooling and power generation.

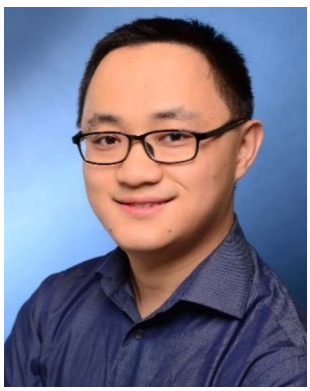

Ran He

Ran He has led a research group at the Leibniz Institute for Solid State and Materials Research at IFW Dresden, Germany, since 2020. He earned his PhD degree from the University of Houston in 2016. He then worked as a postdoctoral researcher at the Leibniz Institute for Solid State and Materials Research at IFW Dresden. He led a German Research Foundation (DFG) project and was awarded a European Research Council Starting Grant in 2023. His research focuses on electronic and phononic structures of solids, semiconductor energy materials, and nonequilibrium synthesis of thermoelectric materials.

technology. For several decades, the pursuit of this objective has primarily depended on Bi_2Te_3-based thermoelectric materials. Nevertheless, Te, the essential constituent element of these compounds, is both scarce[12] (Fig. 1A) and environmentally hazardous, which substantially constrains their further development and large-scale deployment. Until recently, attributed to the unparalleled advantages of excellent thermoelectric performance, earth-abundant constituent elements,[12] environmental friendliness, and favorable mechanical stability,[13–16] Mg-based thermoelectric devices, comprising p-type MgAgSb and n-type $Mg_3(Bi, Sb)_2$, have emerged as promising next-generation candidates to replace commercial Bi_2Te_3.[13,14,16–20] Of particular significance, MgAgSb achieves a markedly higher figure of merit (*ZT*) than other thermoelectric materials in the 400–600 K temperature range[21–34] (Fig. 1B), underscoring its unique and indispensable role. Consequently, MgAgSb-based power generation devices deliver unmatched performance under temperature differences of ~300 K (ref. 13 and 35–47) (Fig. 1C). However, compared with other advanced energy conversion technologies, such as solar cells,[48,49] the primary obstacle limiting the widespread commercialization of thermoelectric devices is their relatively low conversion efficiency, which originates from the intrinsically low *ZT* of the materials. Theoretically, achieving high thermoelectric performance requires simultaneously optimizing electronic transport while suppressing thermal transport.[50,51] However, the strong coupling between charge carriers and phonons fundamentally constrains the ability to independently tune these properties, thereby hindering the realization of significantly higher *ZT* values. To address these, substantial progress has been made in enhancing the performance of MgAgSb through strategies such as microstructure engineering,[14,16,17,52,53] composite material optimization,[15,54] and advanced synthesis technologies,[13,14,53,55–59] which have been partially summarized and discussed in several reviews.[60–63] Concurrently, device-level advancements have focused on thermoelectric interface materials (TEiMs) design,[64–69] module geometry optimization,[18,68] and investigations into operational stability.[70] These

Jiehe Sui

Jiehe Sui is a professor at the School of Materials Science and Engineering, Harbin Institute of Technology. He received his PhD degree from Harbin Institute of Technology in 2006. From 2013 to 2015, he served as a visiting scholar at the University of Houston, USA. He received the funding of the 2016 National Natural Science Fund for Excellent Young Scientists. His research focuses on thermoelectric materials optimization and thermoelectric device fabrication, particularly for energy conversion applications. To date, he has authored over 260 SCI-indexed papers, including Science, Joule, and Nature Communications.

Kornelius Nielsch

Kornelius Nielsch has been Director of the Institute for Metallic Materials (IMW) at the Leibniz Institute for Solid State and Materials Research Dresden (IFW) since 2015, where he leads a research group working on sustainable thermoelectric materials and devices for thermoelectric cooling. Professor Nielsch received his diploma in physics from the University of Duisburg in 1997 and his PhD in physics from Martin Luther University Halle-Wittenberg, Germany, in 2002. From 2002 to 2003, he was a postdoctoral fellow at MIT after which he took up the position of group leader at the Max Planck Institute for Microstructure Physics in Halle, Germany, in 2003. Kornelius Nielsch then moved to the Institute of Applied Physics at the University of Hamburg, where he was Professor of Experimental Physics from 2007 to 2015. From 2009 until 2015, he has coordinated the Priority Program on Nanostructured Thermoelectrics, and he is currently coordinating the Marie Curie Doctoral Network on Mg-based alloys for thermoelectric cooling in collaboration with 15 partner institutions across Europe.

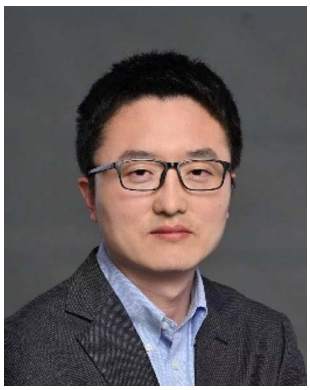

Zihang Liu

Zihang Liu is a full professor at the School of Materials Science and Engineering, Harbin Institute of Technology. He received the funding of the 2021 National Natural Science Fund for Excellent Young Scientists (Overseas). He completed his PhD in materials science and engineering at the Harbin Institute of Technology. He worked as a postdoctoral fellow at the University of Houston, USA, and the National Institute for Materials Science, Japan, from March 2017 to August 2021. His research interests include thermoelectric materials and devices, DFT calculations, as well as flexible materials for applications in energy conversion and storage. As the first author or corresponding author, he has published over 50 papers in high-quality journals, including Science, Joule, Nature Communications, and Proceedings of the National Academy of Sciences of the United States of America, with a total number of citations exceeding 8000.

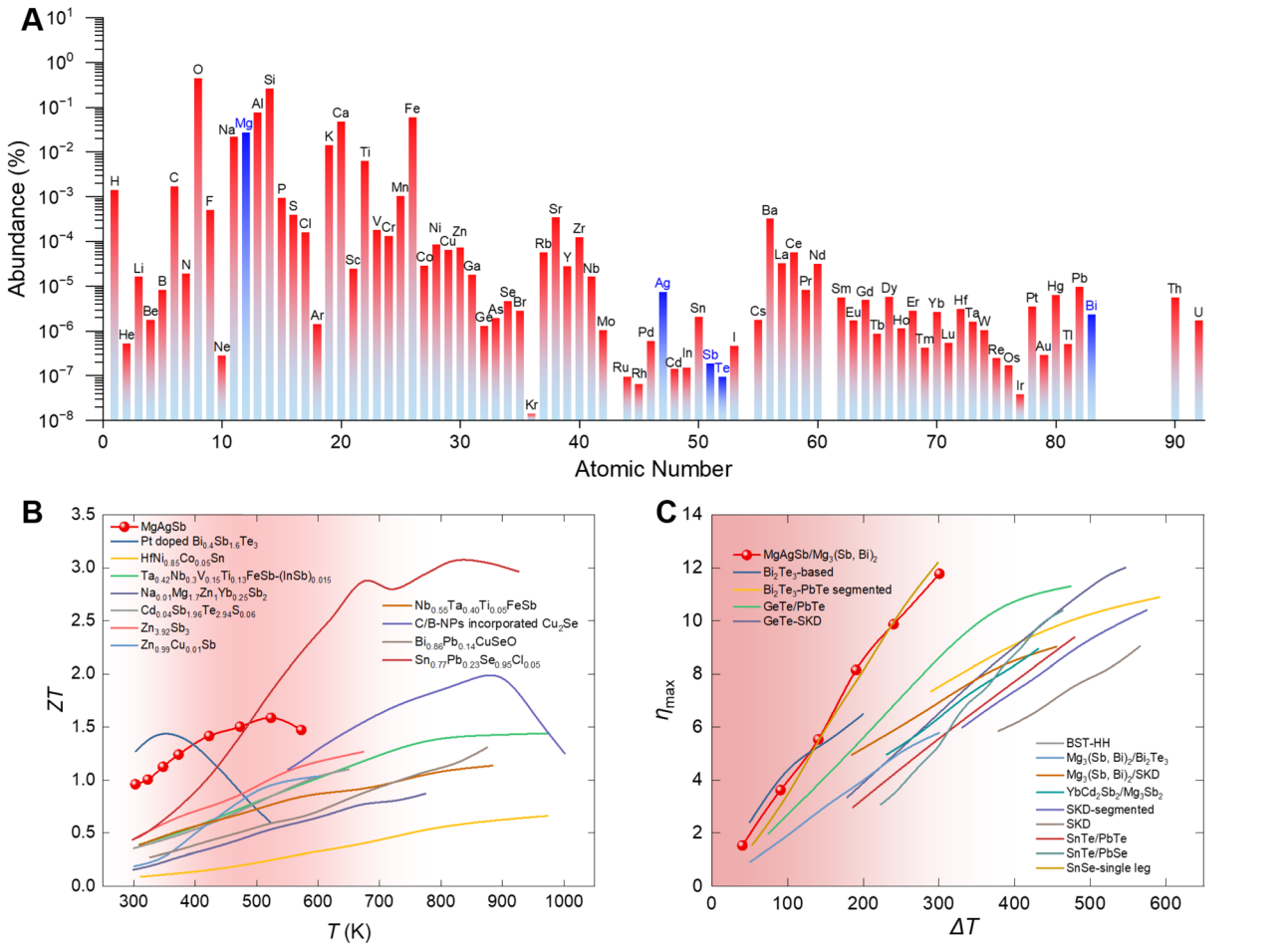

Fig. 1 (A) Abundance of elements in Earth's crust.[12] (B) Temperature-dependent *ZT* of MgAgSb, benchmarked against representative and high-performance p-type thermoelectric materials in the range of 300–1000 K.[21–34] (C) Comparison of the maximum conversion efficiency of MgAgSb-based modules with representative state-of-the-art single-stage and segmented thermoelectric modules.[13,35–47]

developments have profound implications not only for the thermoelectric field but also for other functional material systems. MgAgSb research offers valuable insights into the synthesis of challenging materials and provides innovative ideas for interface material design, particularly concerning the electrical properties of semiconductor materials. Given its broad relevance, a comprehensive and generalized review of these advancements is essential. In the first section of this review, we provide a comprehensive overview of recent advances in the fundamental understanding and property optimization of MgAgSb, encompassing intrinsic electronic and thermal transport characteristics, state-of-the-art synthesis and processing strategies, and the pivotal role of defect engineering in tailoring performance. The second section is devoted to progress in the development of thermoelectric power generation and cooling devices, with particular emphasis on innovations in TEiM design, device geometry optimization, and long-term operational stability. Finally, we critically assess the remaining scientific and technological challenges and present an outlook on prospective research directions and opportunities for the future advancement of MgAgSb-based thermoelectrics.

2 Advances in thermoelectric performance optimization of MgAgSb

2.1 Understanding the structural complexity and phase evolution in MgAgSb

As early as 1941, Nowotny and Sibert elucidated the crystal structure of MgAgSb *via* X-ray diffraction (XRD) analysis, establishing its structural analogy to MgCuAs, with both adopting a tetragonal Cu_2Sb-type configuration.[71] Subsequent investigations employing variable-temperature XRD by Kirkham *et al.* and variable-temperature synchrotron radiation by Mi *et al.* systematically resolved the temperature-dependent structural evolution of MgAgSb, revealing the existence of three distinct phases.[72,73] The high-temperature γ-MgAgSb phase adopts a conventional half-Heusler structure, isostructural with MgCuSb, wherein the Mg–Sb framework forms a NaCl-type rock-salt sublattice and Ag atoms occupy half of the octahedral interstices; it crystallizes in the space group $F\bar{4}3m$, contains 16 atoms per unit cell, and exhibits a theoretical density of 5.61 g cm^{-3} (Fig. 2A). The intermediate-temperature β-MgAgSb phase adopts a tetragonal Cu_2Sb-type lattice (space group *P4/nmm*) with 6 atoms per unit cell, a theoretical density

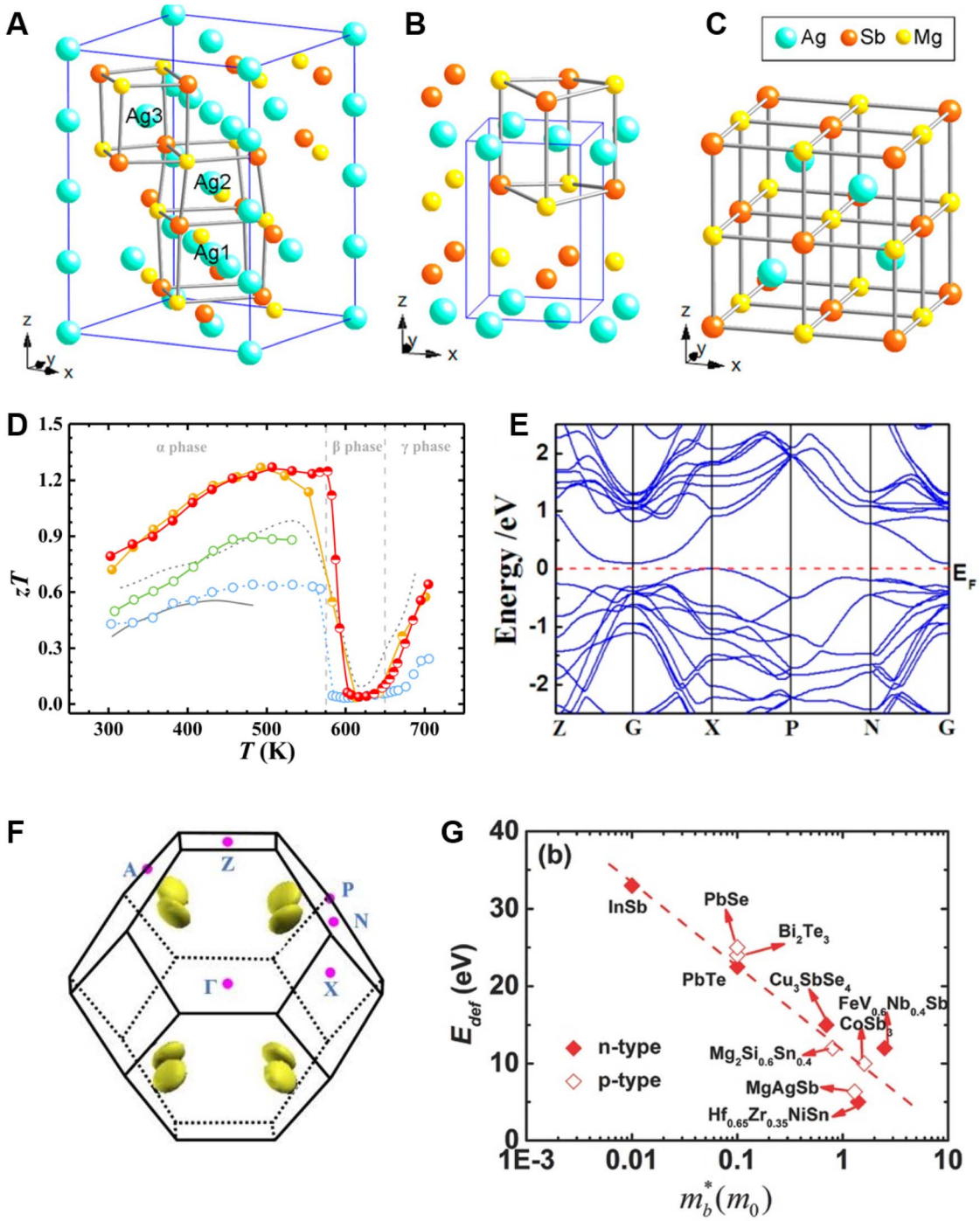

Fig. 2 Crystal and band structure of MgAgSb. (A–C) are crystal structures of α-MgAgSb, β-MgAgSb, and γ-MgAgSb, respectively.[72] (D) Temperature dependence of the *ZT* value of MgAgSb with different phase structures.[74] (E and F) are the band structure and the corresponding first Brillouin zone of α-MgAgSb,[75] respectively. (G) Effective mass dependence of deformation potential.[76] (A–C) Adapted with permission from ref. 72. © 2017 American Chemical Society. (D) Adapted with permission from ref. 74. © 2023 Acta Materialia Inc. (E and F) Adapted with permission from ref. 75. © 2015 American Chemical Society. (G) Adapted with permission from ref. 76. © 2016 WILEY-VCH Verlag GmbH & Co. KGaA, Weinheim.

of 6.26 g cm^{-3}, and metallic character (Fig. 2B). The low-temperature α-MgAgSb phase is a distorted half-Heusler variant, in which the Mg–Sb rock-salt sublattice undergoes a 45° rotation about the *c*-axis; it crystallizes in the space group $I\bar{4}c2$, contains 48 atoms per unit cell, and has a theoretical density of 6.31 g cm^{-3} (Fig. 2C). With increasing temperature, MgAgSb undergoes structural evolution with critical phase-transition points. The *ZT* value drops sharply when MgAgSb transforms into the β phase due to its metallic electronic structure, and then gradually rises again once the temperature exceeds the β–γ phase transition (Fig. 2D). As a result, the practical operating temperature window of MgAgSb is largely

confined to the lower-temperature region around 300 °C. More critically, the pronounced structural complexity of MgAgSb results in an intrinsically low solubility for most extrinsic dopants, which in turn renders its phase-transition temperature insensitive to doping. This characteristic further limits the manipulation of phase transition temperature and the potential application of MgAgSb at elevated temperatures.

Ying *et al.* computed the electronic band structure and density of states of α-MgAgSb using density functional theory (DFT) within the VASP framework, revealing that MgAgSb is an indirect, narrow-bandgap semiconductor with $E_g \approx 0.26$ eV.[75] The valence band maximum is located at the X point, while the conduction band minimum lies at the G point (Fig. 2E). Notably, the material exhibits a high band degeneracy ($N_v = 8$; Fig. 2F), and the flatness of the valence band maximum confers a large single-band effective mass, contributing to an enhanced Seebeck coefficient. Using the Bardeen–Shockley deformation potential theory, Liu *et al.* determined that MgAgSb possesses a low deformation potential (Fig. 2G), indicative of weak electron–phonon coupling.[76] This characteristic, coupled with its structurally induced complexity, enables unusually high carrier mobility. The synergistic interplay of high band degeneracy, large effective mass, and small deformation potential underpins the excellent electrical transport performance of MgAgSb.

To investigate the intrinsic mechanism underlying the low thermal conductivity of MgAgSb, Ying *et al.* theoretically and experimentally confirmed the coexistence of both global and local weak chemical bonds in α-MgAgSb, revealing that low-frequency optical phonon vibrations with "rattling-like" thermal damping are the primary origin of its reduced lattice thermal conductivity.[77] Liu *et al.* elucidated the mechanism behind the low lattice thermal conductivity of MgAgSb through DFT calculations, identifying factors such as weak chemical bonding, strong anharmonic coupling between the longitudinal acoustic branch and the longitudinal optical branch, and high anharmonic behavior in the longitudinal acoustic branch (Fig. 3A and B).[78] Li *et al.* employed neutron scattering experiments alongside *ab initio* calculations to demonstrate that the ultralow lattice thermal conductivity of MgAgSb arises primarily from the strong scattering of transverse phonons by the distorted Mg–Sb rock-salt sublattice.[79] Consequently, longitudinal phonons dominate the heat transport and thus principally

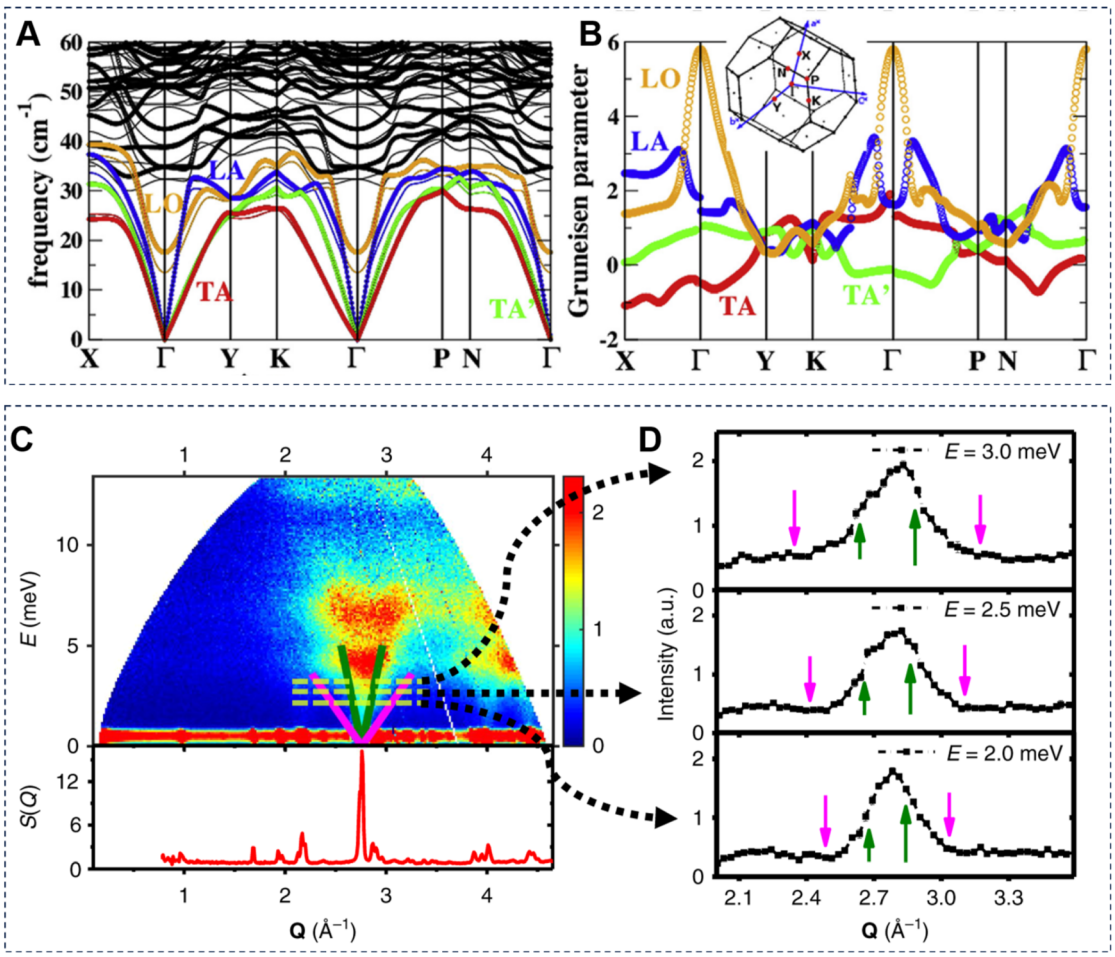

Fig. 3 Mechanism of low lattice thermal conductivity of MgAgSb. (A) Calculated phonon dispersion curves and (B) the corresponding Grüneisen parameter spectra for MgAgSb.[78] (C and D) are measured Bose-factor-calibrated dynamic structure factor $B(Q, E)$ and the corresponding neutron-weighted *ab initio* calculated $B(Q, E)$ pattern.[79] (A and B) Adapted with permission from ref. 78. © 2017 Acta Materialia Inc. (C and D) Reproduced from ref. 79 under the terms of the Creative Commons Attribution 4.0 International License (CC BY 4.0).

determine the κ_{lat} value. Moreover, observed phonon softening further elucidates the anharmonic nature of the atomic vibrations within the lattice (Fig. 3C and D).

2.2 Synthesis strategies for enhancing thermoelectric properties

Since Kirkham *et al.* first reported and systematically investigated the promising thermoelectric properties of MgAgSb in 2012,[73] efforts to optimize its thermoelectric performance have mainly focused on refining preparation and synthesis methods to improve phase purity, owing to its intrinsically distorted crystal lattice and complex phase composition. The low formation energy of Ag_3Sb is one of the key factors responsible for its easy formation in MgAgSb, which in turn degrades thermoelectric performance. To address this challenge, in 2014, Zhao *et al.* introduced a two-step ball-milling strategy to avoid the direct contact and reaction between Ag and Sb raw materials, thereby producing MgAgSb with significantly enhanced phase purity. The *ZT* of the resulting MgAgSb reached 0.7 at room temperature, with an average *ZT* of 1.1.[80] Since then, high-energy ball-milling mechanical alloying has become the predominant approach for MgAgSb synthesis. Subsequently, extensive investigations were conducted on carrier regulation through element doping to optimize MgAgSb performance,[60,76,78,81–87] systematically evaluating the effectiveness of different dopants and the impact of doping at various lattice sites on carrier mobility. Zhang *et al.* further improved the two-step ball-milling process by enhancing milling efficiency and reducing impurity phases.[13,14,53] In the high-energy ball-milling mechanical alloying process, they replaced the traditional V-belt with a timing belt to increase the rotational speed and used tungsten carbide balls to increase the collision energy (Fig. 4A), thereby significantly improving the purity of the ball-milled powder. Subsequent high-temperature annealing facilitated substantial grain growth (Fig. 4B and C), which enhanced carrier mobility and power factor. Under this synthesis approach, the resulting MgAgSb exhibited a ZT_{ave} of 1.4 in the temperature range of 300–573 K.

The thermoelectric properties of MgAgSb are highly sensitive to multiple synthesis parameters, including the ball-milling process, raw material particle size, composition, sintering temperature, and applied pressure during sintering, which collectively contribute to the variations in material properties reported by different researchers. Boor *et al.* systematically investigated the factors influencing MgAgSb performance during synthesis. By comparing traditional planetary ball milling with high-energy ball milling, they demonstrated that high-energy ball milling more readily yields MgAgSb with lower impurity-phase content and identified Ag_3Sb as the primary impurity responsible for deteriorated thermoelectric performance.[57] Further studies on the influence of MgAg precursors on the final MgAgSb synthesis revealed that the quality of MgAg produced in the first ball-milling step critically determines the performance of the final MgAgSb. The particle sizes of Mg and Ag were found to strongly influence the quality of the MgAg precursor. To address this, a sintering step was incorporated after the initial MgAg ball milling to improve precursor quality and reduce the Ag_3Sb impurity content, resulting in a peak *ZT* of approximately 1.2 at 500 K.[56] Moreover, the Boor research group established clear synthesis–composition–property relationships (Fig. 4D), enabling the reproducible preparation of high-performance MgAgSb (ZT = 1.34 at 561 K).[55] They also reported that, within the Mg–Ag–Sb phase diagram, the homogeneity range for MgAgSb is extremely narrow (<0.1 at%), meaning that the TE performance of MgAgSb is highly sensitive to impurity phases, primarily due to their adverse effect on carrier mobility. Other notable findings include: cleaning the ball-milling jar after the first milling step improves performance reproducibility; secondary phases such as Mg_3Sb_2 and Sb exert only a minor influence on the TE performance of

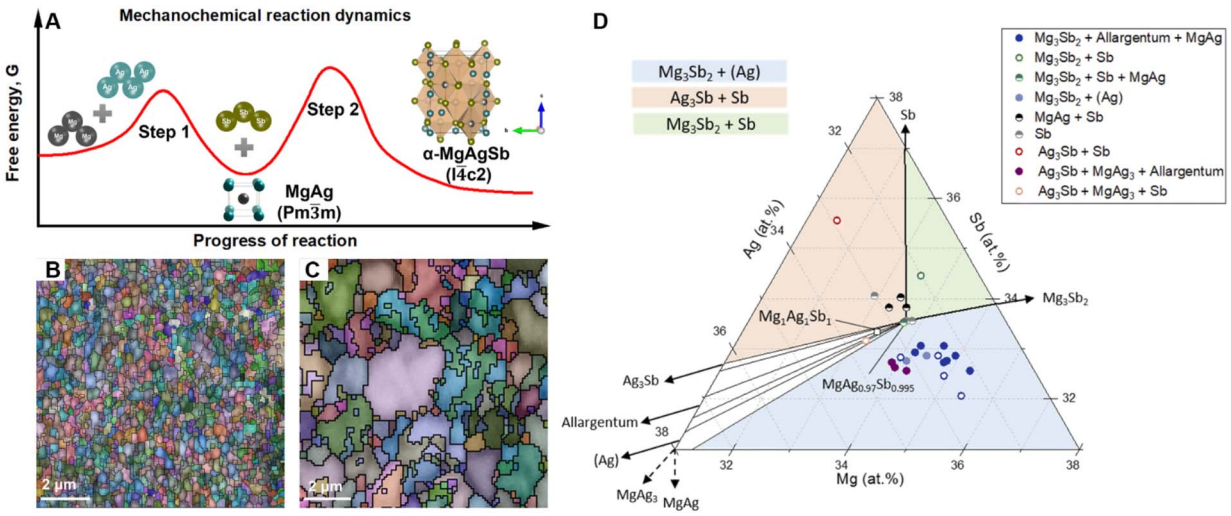

Fig. 4 Progress in MgAgSb synthesis. (A) Schematic of the reaction mechanism for the two-step ball-milling synthesis. (B and C) are EBSD images of as-synthesized and post-annealed α-MgAgSb samples, respectively.[13] (D) Mg–Ag–Sb phase diagram at 300 °C with the positions of samples plotted based on their measured effective compositions.[55] (A–C) Adapted with permission from ref. 13. © 2024 Published by Elsevier Inc. (D) Reproduced from ref. 55 under the terms of the Creative Commons Attribution 3.0 International License (CC BY 3.0).

MgAgSb, whereas Ag and Ag_3Sb substantially degrade performance. Additionally, the intense cold welding of the powders during the ball milling process of MgAgSb was identified as the main cause of impurity formation, since it hindered contact and reaction between the raw materials and the fractured powders. To address this issue, Li *et al.* introduced stearic acid, a classical ball-milling aid, into MgAgSb. By reducing the extent of cold welding, sufficient milling was achieved with significantly less time. As a result, the required ball milling duration was shortened from the conventional 20 hours to only 5 hours, while maintaining high performance and greatly reducing lattice thermal conductivity.[88]

Although two-step high-energy ball milling proved to be the most successful means of synthesizing high-performance MgAgSb, this process is very time-consuming and labor-intensive, and is one of the most significant limiting factors preventing the replacement of commercial Bi_2Te_3 by MgAgSb for large-scale applications. Aiming for a faster and scalable fabrication route, Ying *et al.* used the high-temperature melting method to prepare MgAgSb.[75] To eliminate impurity phases during long-term annealing at the phase transition temperature, indium (In) was used to replace antimony (Sb) to further optimize the carrier concentration. Ultimately, the prepared samples achieved a *ZT* peak value of 1.1 at 525 K. Similarly, Huang *et al.* utilized high-temperature melting and low-temperature annealing of Ta tubes to achieve higher-quality pure MgAgSb with larger grain sizes and lower oxygen content than those produced by high-energy ball milling.[74] They obtained an average power factor of 25 $\mu W\ cm^{-1}\ K^{-2}$ and an average *ZT* value of 1.1 in the temperature range of 300 to 550 K. The comparable *ZT* achieved by the high-temperature melting method make competitive alternative to high-energy ball milling. However, the specific techniques of Ta tube limit the large-scale materials production for practical applications.

2.3 Defect engineering and composite strategy optimization

In thermoelectric materials, defect structures are deliberately engineered to achieve the selective scattering of charge carriers and phonons, thereby enhancing the overall figure of merit. In the case of MgAgSb, both computational and experimental studies have consistently identified Ag vacancies, an intrinsic defect, as the dominant factor responsible for its inherent p-type semiconductor behavior.[83,89,90] Moreover, a high concentration of Ag vacancies plays a crucial role in suppressing lattice thermal conductivity. Liu *et al.* demonstrated that Ag vacancies are highly sensitive to the sintering temperature, enabling the precise tuning of carrier concentration and the power factor through controlled thermal processing.[83] Given the high volatility of Mg, Li *et al.* extended these investigations to Mg–Ag antisite defects and their tunability.[17] Experimental observations revealed the presence of Mg–Ag antisite defects within the lattice, forming interconnected nanoscale regions embedded in the matrix. This unique microstructural feature serves as an efficient phonon-scattering network while largely preserving carrier transport pathways. To further promote the formation of such defects, Zn doping was employed to reduce their formation energy. This strategy effectively suppressed the Ag-rich secondary phase, enhanced phonon scattering, and improved carrier mobility, thereby lowering the lattice thermal conductivity. As a result, an average *ZT* of approximately 0.75 was achieved in the low-temperature range of 200–400 K. Building upon defect engineering, Xie *et al.* realized an ultralow lattice thermal conductivity by constructing multi-scale structural defects in α-MgAgSb through high-energy ball milling followed by low-temperature sintering.[16] The resulting microstructure, comprising ultrafine nanocrystals, high-density dislocations, and randomly distributed micro- and nanopores, facilitated multi-scale phonon scattering (Fig. 5A–C), yielding a lattice thermal conductivity as low as $0.46\ W\ m^{-1}\ K^{-1}$ at 300 K, surpassing the typical lower bound for such materials. Although this approach caused a slight reduction in electrical performance, it produced an unprecedented *ZT* of ~0.94 at 300 K and an average *ZT* of ~1.16 over the range from room temperature to 473 K. In a complementary approach, Liao *et al.* exploited sintering pressure as a means to regulate the size of micropores within MgAgSb, thereby achieving an optimal trade-off between carrier mobility and lattice thermal conductivity.[52] Samples processed at 80 MPa exhibited a high room-temperature mobility of $87.7\ cm^2\ V^{-1}\ s^{-1}$ and a low lattice thermal conductivity of $0.452\ W\ m^{-1}\ K^{-1}$ at 423 K, resulting in an average *ZT* of 1.11 across the temperature range of 323–573 K. As different defects exhibit different dimensions and sizes, their phonon-scattering behaviors are related to the phonon wavelengths they interact with. For example, Ag vacancies and Mg–Ag antisite defects primarily scatter high-frequency phonons, thereby suppressing the lattice thermal conductivity at elevated temperatures. To achieve phonon scattering across the entire frequency spectrum, constructing hierarchical (multi-scale) defect structures becomes essential, which has already been demonstrated in the work of Xie *et al.*[16]

Using a rapid microwave-assisted synthesis approach, Xin *et al.* incorporated SnTe nanoinclusions into the MgAgSb matrix, which significantly enhanced the Seebeck coefficient by effectively suppressing the bipolar effect.[54] Simultaneously, the introduction of a multiscale hierarchical architecture markedly reduced the lattice thermal conductivity (Fig. 5D–F). Consequently, MgAgSb containing 3 at% SnTe exhibited a 53% increase in *ZT* (~1.0 at 548 K) compared with pristine MgAgSb. Building on the carrier injection effect associated with metal–semiconductor ohmic contacts, Xie *et al.* introduced homogeneously distributed *in situ* MgCuSb nanoprecipitates within the MgAgSb matrix to optimize the carrier concentration of MgCuSb/MgAgSb composites (Fig. 5G–I), thereby decoupling interdependent electronic transport parameters.[15] This strategy yielded a record-high average power factor (PF_{ave}) of 27.2 $\mu W\ cm^{-1}\ K^{-2}$ for $MgCu_{0.1}Ag_{0.87}Sb_{0.99}$ in the temperature range of 300–550 K, surpassing all previously reported values for the MgAgSb system and approaching those of classical Bi_2Te_3-based materials. On this basis, Jiao *et al.* examined the high-temperature stability of MgAgSb and found that prolonged annealing at 548 K induced the formation of significant amounts of Ag_3Sb secondary phase, which increased thermal conductivity and reduced the Seebeck coefficient, thereby

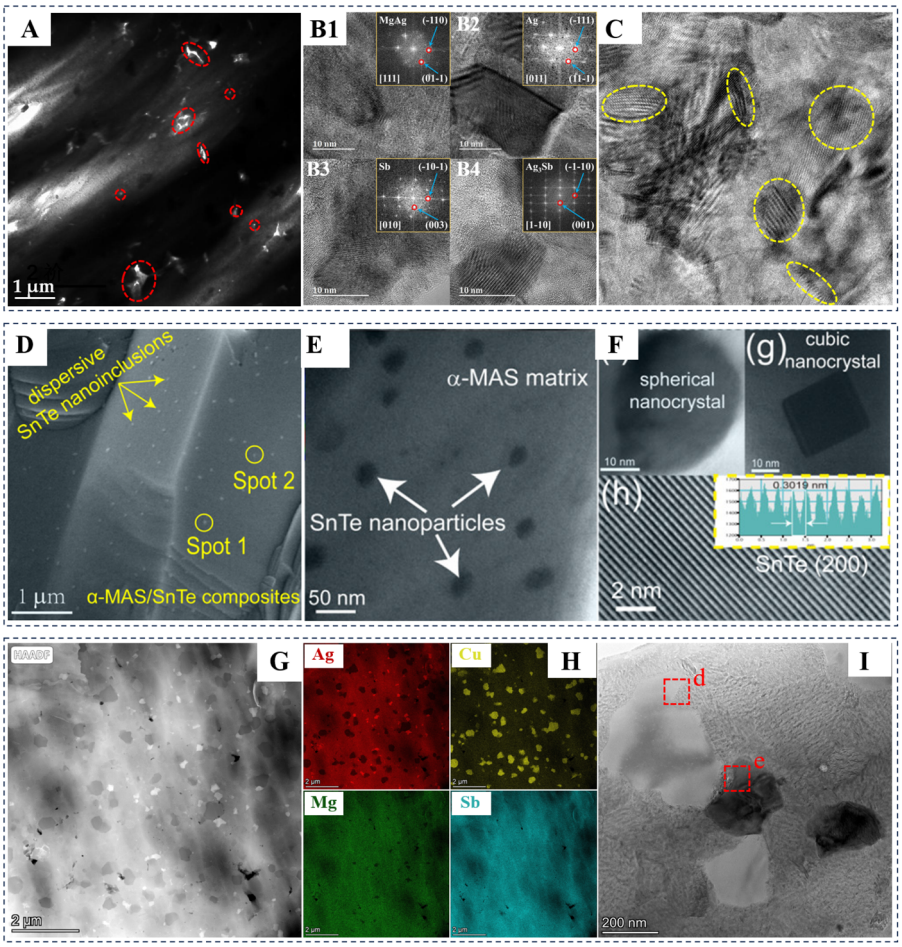

Fig. 5 TEM images showing defects and second-phase inclusions in MgAgSb. (A–C) Show pores ranging from several tens to hundreds of nanometers, nanophases with an average size of ~20 nm, and dense, twisted Moiré fringes and crystal distortions at the interfaces between the matrix and nanoprecipitates.[16] (D–F) Show homogeneously dispersed SnTe nanoparticles and their morphologies.[54] (G–I) Show uniformly distributed nanoprecipitates in the MgAgSb matrix.[15] (A–C) Adapted with permission from ref. 16. © 2023 Elsevier Ltd. (D–F) Adapted with permission from ref. 54. © 2019 American Chemical Society. (G–I) Adapted with permission from ref. 15. © 2024 Wiley-VCH GmbH.

severely degrading *ZT*.[91] To counteract this, Cu enrichment at grain boundaries was employed to lower grain-boundary energy, enabling both thermodynamic and kinetic stabilization of the nanostructure. As a result, the final compound remained thermally stable after 14 days of annealing at 548 K.

3 Progress in MgAgSb-based thermoelectric devices

3.1 Developed interface materials

For thermoelectric (TE) devices, overall conversion efficiency and cooling performance depend not only on the intrinsic TE properties of the bulk materials but also on the performance of the interfacial materials. Pei *et al.* calculated the relationship between interfacial resistivity (ρ_c) and conversion efficiency, showing that efficiency decreases sharply as ρ_c increases.[92–95] Thus, minimizing ρ_c is essential for achieving high conversion efficiency. Equally important is the thermal and chemical stability of the interface, particularly for TE power-generation modules, whose hot-side junctions operate continuously at elevated temperatures. Such conditions provide sufficient energy for atomic reactions and diffusion across the joining interface.[96–99] In these environments, high-reactivity electrode materials (*e.g.*, Cu) and solders (*e.g.*, Sn, Ag, Cu alloys) can diffuse into the TE material, severely degrading its performance because semiconductors are highly sensitive to trace amounts of impurity elements.[100,101] Therefore, in addition to achieving a low ρ_c, ensuring high interfacial stability is critical, especially for TE power-generation applications.

Over the past several years, the selection strategy of TEiM in the TE region has undergone considerable development, and interestingly, the TEiM of MgAgSb is exactly a typical representative case study. Initially, trial-and-error methods were used to choose a metal with a familiar coefficient of thermal expansion (CTE) of TE materials as TEiM. For MgAgSb, Kraemer *et al.*[69] selected Ag as the TEiM of MgAgSb due to the comparable CTE ($\sim 20 \times 10^{-6}$ K^{-1}) and showed a relatively low interfacial resistivity of ~10 μΩ cm^2 (Fig. 6A and B). This value is within an acceptable range. Moreover, the excellent wettability and native low resistivity of Ag make it the most used TEiM of

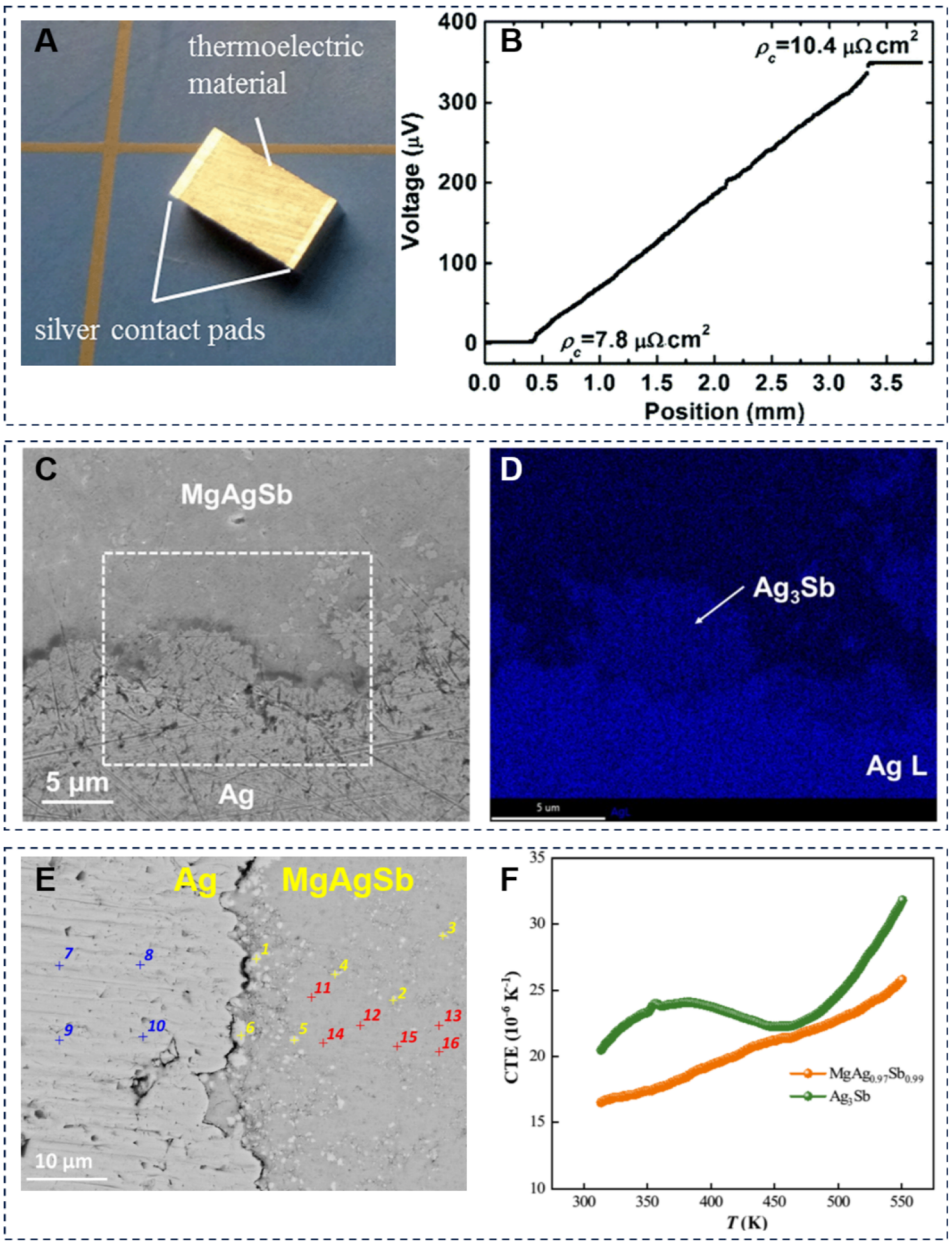

Fig. 6 Stability of Ag as TEiM for MgAgSb. (A) Photograph of MgAgSb thermoelectric single leg incorporating an Ag TEiM.[69] (B) Interface contact resistivity of Ag/MgAgSb junction. (C and D) SEM and corresponding EDS mapping at the Ag/MgAgSb interface after operation.[18] (E) Ag/MgAgSb interface structure after annealing at 553 K for 12 hours.[68] (F) Temperature dependence of the coefficient of thermal expansion (CTE) of Ag_3Sb and MgAgSb. (A and B) Adapted with permission from ref. 69. © The Royal Society of Chemistry 2015. (C and D) Reproduced from ref. 18 under the terms of the Creative Commons Attribution 3.0 International License (CC BY 3.0). (E and F) Adapted with permission from ref. 68. © 2023 The Authors, exclusive licensee American Association for the Advancement of Science.

MgAgSb for a long while. Ying *et al.*[18,102] and Liu *et al.*[103] all selected Ag as TEiM of MgAgSb to fabricate the TE power generation and cooling device and obtain high conversion efficiency and maximum temperature difference. However, the conversion efficiency of the MgAgSb/$Mg_3Sb_{0.7}Bi_{1.3}$ device that takes Ag as TEiM shows a great reduction after long-term operating at 523 K. The formed Ag_3Sb at the Ag/MgAgSb interface is considered to be a potential cause (Fig. 6C and D). Subsequent aging experiments of the Ag/MgAgSb interface conducted by Xie *et al.* suggested that ρ_c of the Ag/MgAgSb interface will dramatically increase to even ~1000 μΩ cm^2 after aging at ~553 K for just 12 hours.[68] The formation of cracks induced by the formation of the impurity phase of Ag_3Sb at the Ag/MgAgSb interface, and the high and varied CTE of Ag_3Sb with temperature, is the main reason (Fig. 6E and F). Similar experimental results were obtained by Zhang *et al.*, and they found that cross section area of TE junctions with TEiM is an important factor that dramatically affects ρ_c of the Ag/MgAgSb interface.[14]

To avoid the high interfacial resistivity caused by chemical reaction at the interface, a high-throughput method for TEiM selection has been proposed by Chen *et al.*,[104] by mixing TEiM candidate alloys into TE materials and then aging the as-sintered bulks at operating temperature for a certain time, the thickness of the interface reaction/diffusion layer (IRL) certified by SEM was indicated to evaluate the interface diffusion and reaction behavior between potential candidates and TE materials, as a select criterion. Wu *et al.* applied such methods to MgAgSb, and AgMg compounds, which were filtered out according to the limited IRL[67] (Fig. 7A and B). After that, tiny Mn was alloyed with AgMg to form $AgMgMn_{0.1}$ for CTE optimization. Benefited from weak interface reaction and matched CTE (Fig. 7C), a high bonding strength of 34.5 MPa and a low contact resistivity of 4.5 μΩ cm^2 were obtained for the $AgMgMn_{0.1}$/MgAgSb interface. Similarly, Zou *et al.* creatively used a high-throughput screening approach to alternately stack ten kinds of metal candidate powders with MgAgSb powders to form bulk samples with a segmented structure by one-step sintering at 573 K.[64] Such a segmented structure allows direct characterization of interfacial resistivity and determines the elemental diffusion and chemical reaction by electrical and elemental analysis scanning across all aged interfaces (Fig. 7D–F). The selected Co/MgAgSb exhibits a low interfacial resistivity of 2.5 μΩ cm^2, high bonding strength of 60.6 MPa, and high thermal stability at 573 K. The interfacial microstructure and calculated interfacial reactions, as well as diffusion behaviors, indicated that the excellent electrical, mechanical, and chemical stability of the Co/MgAgSb junction is mainly attributed to the formation of strong covalent bonds between Co and Sb atoms, thereby maintaining an inert and stable interface.

Although high-throughput methods can effectively select stable and low-resistivity TEiMs, this process entails synthesis, processing, and long-term annealing at elevated temperatures, which is time- and cost-consuming. More importantly, the chemical reaction at the interface could not be easily predicted by the junction during the short-term aging process. Additionally, the limited availability of elements restricts the range of material choices. To address this challenge, Xie *et al.*, taking MgAgSb as a case study from the perspective of the Gibbs energy of the interface structure of TEiM and TE materials, developed a universal TEiM screening strategy based on phase diagram predictions by density functional theory, combining the phase diagram with electrical resistivity and melting points of potential reaction products (Fig. 8).[68] By using the established screen strategy, semimetal MgCuSb as a reliable TEiM for high-performance MgAgSb was discovered. The MgCuSb/MgAgSb junction exhibits low interfacial contact resistivity (1 μΩ cm^2) even after annealing at 553 K for 16 days. Moreover, the university of this TEiM screen strategy was verified in several representative TE materials—Bi_2Te_3, Zn_4Sb_3, $CoSb_3$, and NbFeSb—from room temperature to high temperature.

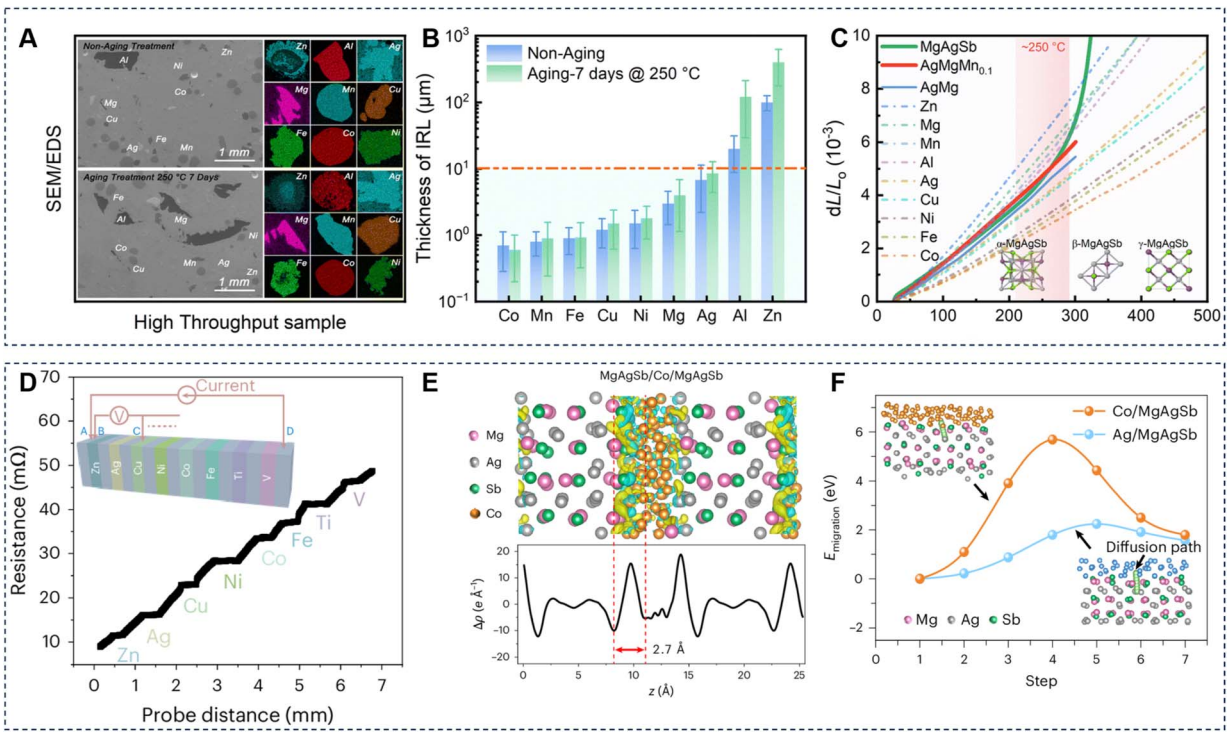

Fig. 7 High-throughput TEiM screening strategy.[64,67] (A) SEM and EDS mapping of high-throughput samples before and after aging treatment. (B) Statistical thickness of the IRL at TEiM/MgAgSb interfaces. (C) Normalized length change ($\Delta L/L_0$) *versus* temperature curves for TEiM and MgAgSb. (D) Segmented sample scan used to measure resistance and simultaneously determine ρ_c of each interface. (E) Charge density difference at the MgAgSb/Co/MgAgSb junction. (F) Energy barrier for Co and Ag atom migration from the interface into MgAgSb. (A–C) Adapted with permission from ref. 64. © The Royal Society of Chemistry 2024. (D–F) Adapted with permission from ref. 67. © The Author(s), under exclusive licence to Springer Nature Limited 2025.

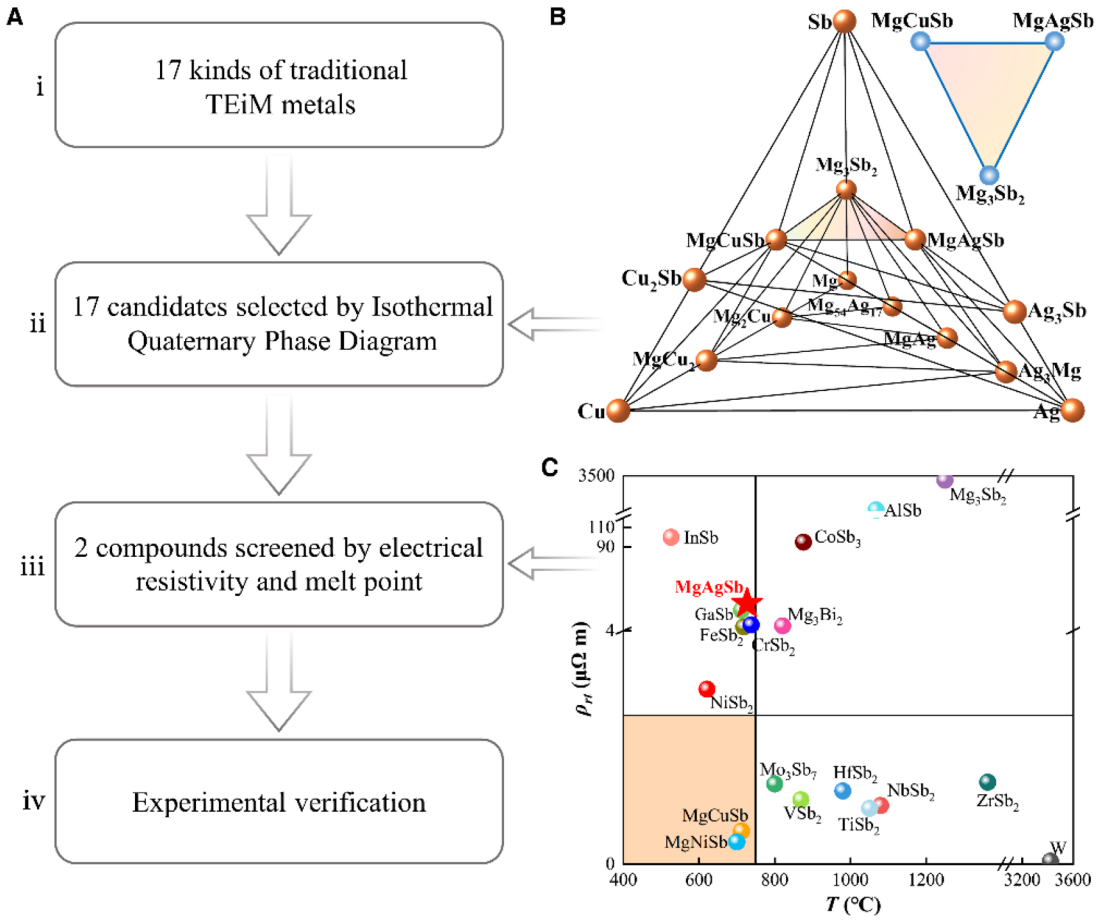

Fig. 8 Established universal TEiM screening strategy.[68] (A) Four-step flowchart of the screening strategy. (B) Phase diagram of Mg–Ag–Cu–Sb. (C) Melt point and room temperature electrical resistivity of selected TEiM candidates. Adapted with permission from ref. 68. © 2023 The Authors, exclusive licensee American Association for the Advancement of Science.

Considering that Sb diffusion from MgAgSb to the TEiM will induce Sb deficiency in MgAgSb and impair the TE performance of MgAgSb. Li *et al.* directly employ Sb as the TEiM in MgAgSb.[65] Specifically, the Sb/MgAgSb junction exhibits a self-optimized ρ_c even exposed to 573 K for 30 days in air (decreasing from 20.8 μΩ cm^2 to 7.9 μΩ cm^2). The structural evolution analysis indicates that Mg diffusion from MgAgSb into the Sb TEiM leads to Mg deficiency and thereby an increased carrier concentration in MgAgSb, which is the main reason for optimized ρ_c. Except for excellent thermal stability and self-optimized ρ_c, low cost and high wettability are two other advantages for large-scale applications and assembly of MgAgSb-based TE module. Based on a similar idea, that is, considering the inherent high chemical reactivity and volatility of Mg,[66] Chen *et al.* developed Mg_2Ni as a unified contact layer for both MgAgSb and $Mg_3(Bi, Sb)_2$. Benefits from comparable CTE between Mg_2Ni and MgAgSb, the Mg_2Ni/MgAgSb junction exhibits an excellent low ρ_c and high reliability. As shown in Fig. 9, the ρ_c of the Mg_2Ni/MgAgSb junction increases from ~1.7 μΩ cm^2 to ~5.1 μΩ cm^2 even after annealing at 573 K for 30 days.

3.2 MgAgSb-based cooling devices

Initially, MgAgSb has long been considered a promising p-type material for power generation. However, it was only recently that n-type $Mg_3(Bi, Sb)_2$ with high performance near room temperature was developed.[106] Consequently, Liu *et al.* combined the $Mg_3(Bi, Sb)_2$ to fabricate an eight-pair Mg-based cooling device for the first time.[19] At a high-temperature end

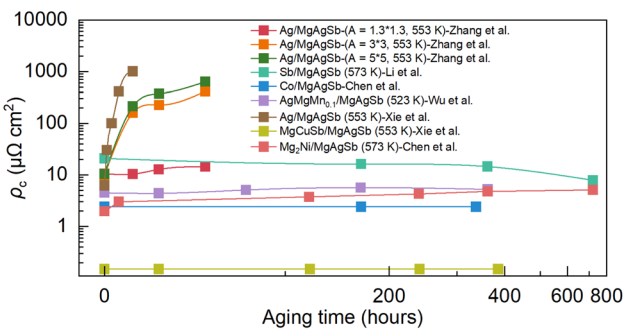

Fig. 9 Evolution of interface resistivity of recently developed TEiMs of MgAgSb with aging time.[64–68,105]

temperature of 325 K, the device achieved a maximum temperature difference of 56.5 K and a maximum cooling power of 3.0 W, demonstrating significant cooling application potential. Xie *et al.* improved the room temperature *ZT* value of MgAgSb by constructing multi-scale defects. The seven pairs of Mg-based devices they constructed achieved a maximum temperature difference of 52 K at the high temperature end of 300 K, and a cooling efficiency coefficient of performance (COP) of 8.3 at a temperature difference of 5 K, which is slightly lower than that of Bi_2Te_3.[16] Thanks to the performance optimization of n-type $Mg_3(Bi, Sb)_2$, the Mg-based device fabricated by Ying *et al.* achieved a maximum temperature difference of 52 K at a high temperature of 302 K.[18] Zhang *et al.* utilized n-type Bi_2Te_3 as the n-type leg and combined it with devices prepared using MgAgSb optimized for near-room-temperature performance, achieving a maximum temperature difference of 60 K at the high-temperature end of 300 K.[14] Another two-pair TE cooling device prepared by Li *et al.*, which consists of MgAgSb and commercial n-type Bi_2Te_3, obtained a temperature difference of 47 K at $T_h = 300$ K.[17] Overall, regardless of whether MgAgSb is combined with n-type $Mg_3(Bi, Sb)_2$ or Bi_2Te_3 to fabricate cooling devices, satisfactory cooling performance can be achieved. However, compared to Bi_2Te_3-based devices, there is still some room for improvement. Therefore, a higher TE cooling performance is anticipated once the TE performance of MgAgSb at room temperature is enhanced.

3.3 MgAgSb-based power generation devices

In 2015, Kraemer *et al.* were the first to investigate the conversion efficiency of single-leg MgAgSb-based thermoelectric devices, reporting a remarkable efficiency of up to 8.5% under a temperature difference of 225 K.[69] This performance exceeded that of conventional Bi_2Te_3-based devices, highlighting the strong potential of MgAgSb as a promising candidate for room-temperature thermoelectric power generation. More recently, advancements in the low-temperature thermoelectric performance of n-type $Mg_3(Bi, Sb)_2$ have paved the way for the fabrication of all-Mg-based multi-leg thermoelectric modules. Following these developments, MgAgSb-based thermoelectric generators have undergone rapid progress, with device-level conversion efficiency improving significantly (Fig. 12). This growth can be attributed to three main factors:

(1) Enhancement of thermoelectric performance in n-type and/or p-type materials. In 2021, Ying *et al.* fabricated the first four-pair Mg-based thermoelectric generator, achieving a maximum conversion efficiency of 7% under a temperature difference of 250 K by integrating segmented n-type $Mg_3(Bi, Sb)_2$ and p-type MgAgSb.[102] Around the same time, Liu *et al.* reported a higher efficiency of 7.3% at a ΔT of 300 K in a seven-pair Mg-based device, enabled by performance-optimized $Mg_3(Bi, Sb)_2$ doped with Cu.[103] Subsequently, Zhang *et al.* achieved a notable conversion efficiency of 12% at 300 K using seven-pair devices constructed with MgAgSb synthesized through an optimized preparation process.[13] From the perspective of practical application, Xie *et al.* further improved device-level performance by tailoring the geometric structure of the module based on power factor enhancement strategies. Their eight-pair Mg-based device delivered a maximum output power of 1.03 W and a peak conversion efficiency of 7.6% at a temperature difference of 300 K.[15]

(2) Development of thermoelectric interface materials (TEiM) for MgAgSb. Reducing interfacial contact resistivity plays a crucial role in minimizing parasitic electrical losses and enhancing overall device performance. Wu *et al.* reported a conversion efficiency of 9.1% and an output power of 0.5 W at a temperature difference of 325 K by employing $AgMgMn_{0.1}$ as a TEiM for MgAgSb.[67] Similarly, Xie *et al.* achieved a conversion efficiency of 9.25% and an output power of 0.53 W at $\Delta T = 300$ K using MgCuSb as the TEiM of MgAgSb.[68] Furthermore, Li *et al.*,[65] Zuo *et al.*,[64] and Chen *et al.*[66] explored alternative TEiMs including Sb, Co, and Mg_2Ni, achieving conversion efficiencies of 8.1% (294 K), 10.2% (287 K), and 10.8% (300 K), respectively.

(3) Optimization of device geometry. It is well established that the p-type and n-type legs in a thermoelectric device typically exhibit different transport properties, which prevents the device from reaching optimal performance under uniform temperature gradients and current conditions. To address this mismatch, careful geometric design is required to maximize device efficiency. However, Ying *et al.* revealed that[107] the large temperature gradient and short distance between the hot and cold ends induced intense thermal radiation and convection during actual operation, which severely disturbed the intended heat flow and resulted in lower conversion efficiency. To mitigate this undesired heat transfer, Ying *et al.* systematically investigated the influence of the fill factor (FF) on device performance. They found that increasing the FF from 16% to 64% led to a significant improvement in conversion efficiency by reducing undesired heat (Fig. 10). This result was subsequently validated by Xie *et al.*, further confirming the critical role of geometric optimization in thermoelectric device design.[68]

In addition to the single-stage module, Xie *et al.* developed a segmented thermoelectric module in which MgAgSb and Mg_3SbBi serve as the low-temperature segment, while n- and p-type skutterudites form the high-temperature segment[108] (Fig. 11). This design was proposed to address the limited operating temperature range of MgAgSb, resulting from its low phase-transition temperature. Owing to the use of proven TEiMs, an optimized geometric design, and an expanded operating temperature window, the module achieved a high conversion efficiency of 12.4% at $T_C = 293$ K and $\Delta T = 540$ K. This work opens a promising avenue for MgAgSb-based thermoelectric devices in medium-temperature waste-heat recovery.

Beyond the extensively investigated n-type $Mg_3(Bi, Sb)_2$, several other low-temperature n-type thermoelectric materials—such as $Bi_{85}Sb_{15}$, $Mg_2(Si, Sn)$, and Ag_2Se—have been coupled with MgAgSb to construct power generation devices. Notably, the $Bi_{85}Sb_{15}$/MgAgSb device developed by Chen *et al.* delivered an output power density of 76.8 mW cm^{-2} and a conversion efficiency of 1.76% within the 200–300 K temperature range.[109] Likewise, Wieder *et al.* reported that a MgAgSb/$Mg_2(Si, Sn)$ device attained a conversion efficiency of 6.4% and an output power of 0.68 W under a temperature gradient of 275

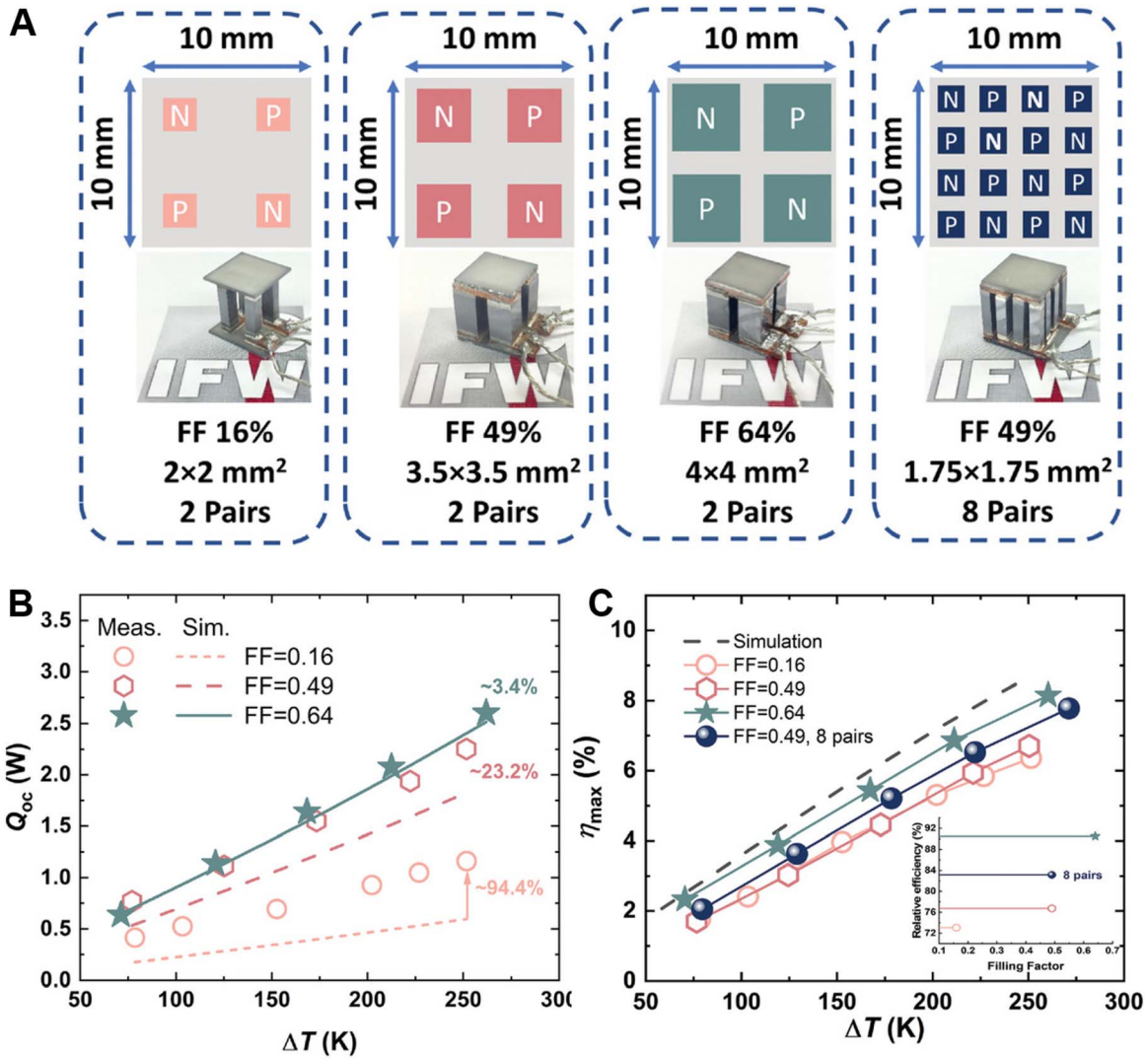

Fig. 10 Impact of the fill factor of the device on thermoelectric performance.[107] (A) The schematics and images of the assembled modules with different filling factors. (B and C) are the temperature difference dependence of heat flow Q and maximum conversion efficiency η_{max} with a changed filling factor. Reproduced from ref. 107 under the terms of the Creative Commons Attribution 4.0 International License (CC BY 4.0).

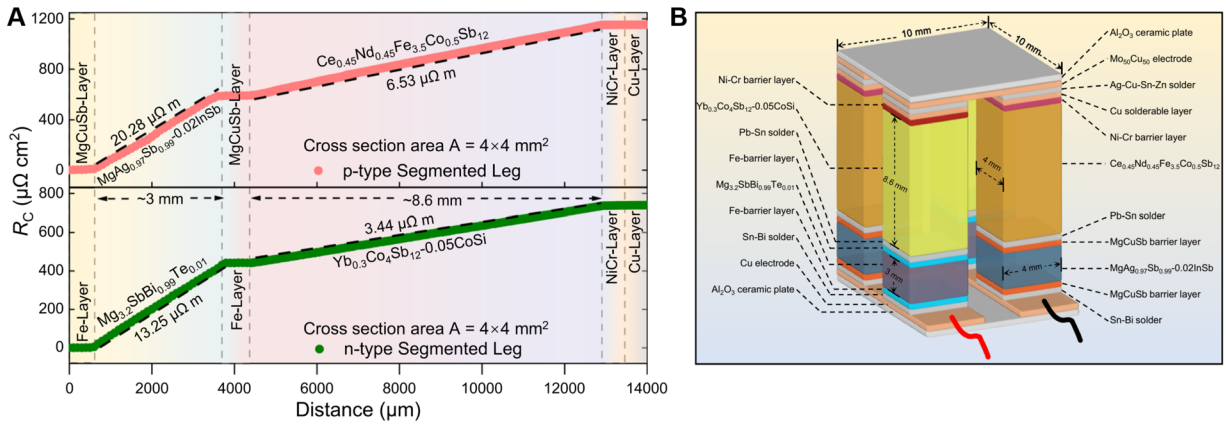

Fig. 11 Schematic diagram of Mg-based and skutterudite segmented thermoelectric power generation module.[108] (A) Measured contact resistivity of n-type and p-type segmented legs. (B) Schematic diagram of a segmented thermoelectric module. Reproduced from ref. 108 under the terms of the Creative Commons Attribution 4.0 International License (CC BY 4.0).

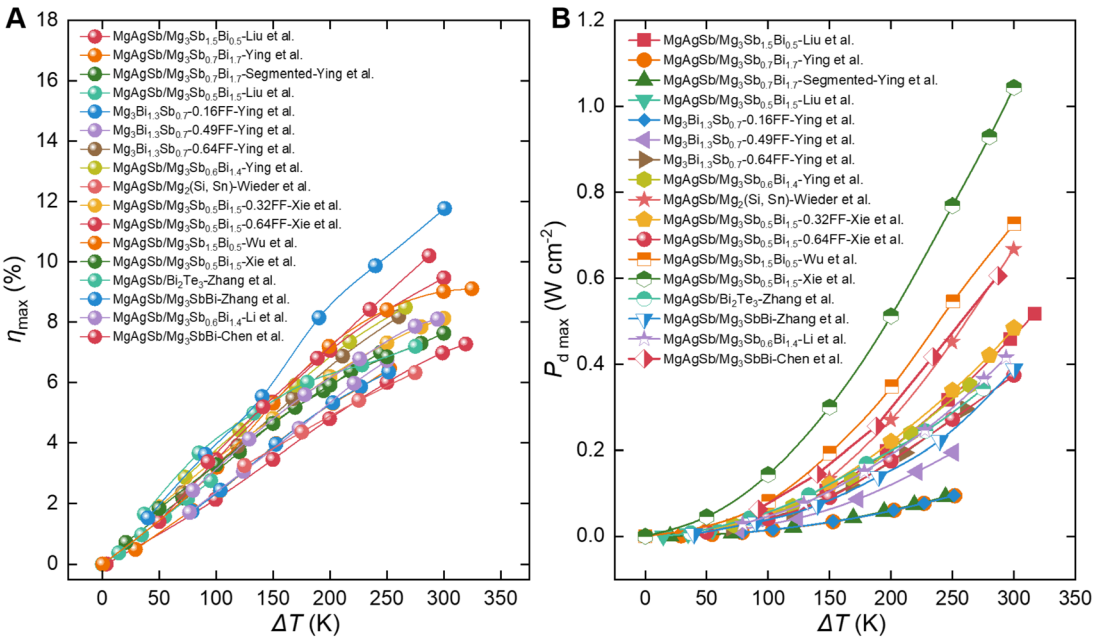

Fig. 12 Power generation performance of MgAgSb-based TE devices.[13–15,18,19,64–68,70,102,103,107,109–111] (A and B) are the temperature difference dependence of maximum conversion efficiency and output power density, respectively.

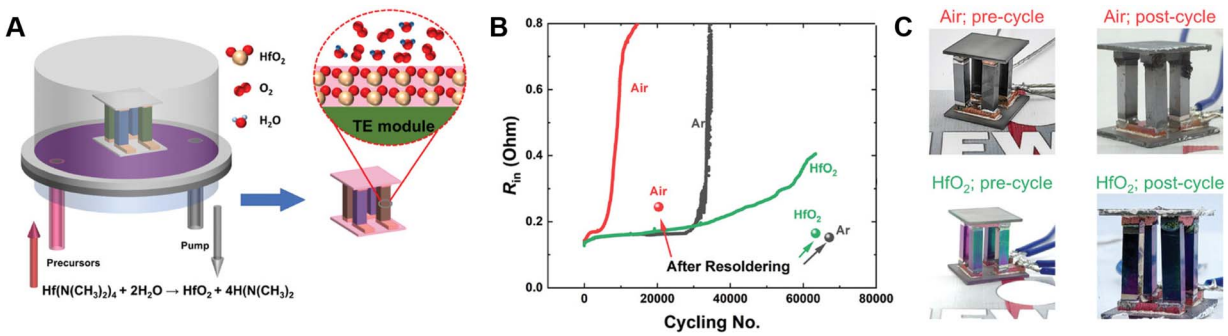

Fig. 13 Investigation on the stability of Mg-based modules.[70] (A) Schematic illustration of the atomic layer deposition (ALD) process and its protective function in thermoelectric modules. (B) Variation in the internal resistance (R_{in}) of modules under thermal cycling. (C) Modules before and after cycling with/without coating. Reproduced from ref. 70 under the terms of the Creative Commons Attribution 4.0 International License (CC BY 4.0).

K.[110] Furthermore, a uni-couple MgAgSb/Ag_2Se system achieved an efficiency of approximately 1.9% at a temperature differential of ~82 K,[112] underscoring the broad applicability and versatility of MgAgSb-based architectures for low-temperature thermoelectric energy harvesting.

3.4 Stability and reliability of MgAgSb devices

Thermoelectric devices are widely regarded as having the potential for exceptionally long service lifetimes, primarily because they perform solid-state energy conversion without relying on moving parts or mechanical motion during operation. This durability is exemplified by the long-term operation of the isotope thermoelectric battery aboard Voyager 1.[113] However, extended operation under high temperature differentials subjects these devices to thermal shocks, temperature-gradient-driven element diffusion, and accelerated interfacial reactions between components. These factors collectively pose serious challenges to the long-term stability of device performance. As a result, degradation over time has become a critical issue, drawing increasing attention in recent research. As previously discussed, the operational stability of thermoelectric devices is principally governed by two factors: the intrinsic thermoelectric properties of the constituent materials and the thermal/electrical resistances at the TEiM-material interfaces. For devices comprising p-type MgAgSb and n-type $Mg_3(Bi, Sb)_2$, Ying *et al.* reported that employing Ag as a barrier layer led to interfacial second-phase formation during operation, thereby increasing interface resistance and causing a ~10% reduction in output power after 32 000 thermal cycles within the 323–500 K range.[18] From a materials standpoint, p-type MgAgSb generally exhibits excellent long-term stability; however, Jiao *et al.* demonstrated that its *ZT* value undergoes slight degradation

during prolonged high-temperature annealing, warranting continued investigation.[91] Conversely, n-type $Mg_3(Bi, Sb)_2$ is well known to be susceptible to reactions with water and oxygen, resulting in diminished thermoelectric performance.[114–116] Their stability, therefore, remains a major concern. Xie *et al.* further revealed that Mg volatilization in $Mg_3(Bi, Sb)_2$ under long-term high-temperature operation in vacuum environments markedly increases internal resistance, thereby reducing device output power.[68] To mitigate such degradation pathways, Ying *et al.* applied an HfO_2 protective coating *via* atomic layer deposition (ALD) to the device (Fig. 11A), which effectively preserved structural integrity, maintaining 93% of the module's initial output power even after re-soldering and approximately 65 000 cycles in air (Fig. 13B).[70] Additionally, extended service testing of Mg-based modules in air underscored the critical role of solder stability in performance retention, highlighting for the first time the necessity of advanced joining technologies to ensure long-term device reliability (Fig. 13C).

4 Summary and outlooks

Following sustained research efforts, the intrinsic crystallographic characteristics and electronic band structure of MgAgSb, together with the fundamental mechanisms governing its high carrier mobility and intrinsically low lattice thermal conductivity, have been comprehensively elucidated. Correspondingly, synthesis methodologies have undergone substantial refinement, encompassing advanced phonon-engineering strategies such as the introduction of multi-scale phonon scattering centers through point defects and hierarchical defect structures, as well as the integration of second-phase composite approaches. These measures have collectively yielded marked enhancements in the PF and/or *ZT*. On the device level, the systematic development of thermoelectric interface materials—drawing on a variety of representative design strategies—has facilitated the fabrication of MgAgSb-based interfaces tailored to diverse operational demands. When combined with optimized geometrical configurations, these advances have enabled the performance of Mg-based thermoelectric generators to significantly outperform those of conventional Bi_2Te_3-based devices within the temperature range of room temperature to 573 K, while Mg-based thermoelectric cooling modules have demonstrated cooling efficiencies on par with their Bi_2Te_3 counterparts. Owing to their abundance of constituent elements, superior mechanical robustness, and promising functional properties, Mg-based thermoelectric materials exhibit substantial potential for broad application. Nonetheless, several critical challenges persist, which presently constrain their full-scale technological deployment.

(1) Cost of raw materials. An often-overlooked limitation lies in the economic burden imposed by the use of silver (Ag) as a constituent element. Despite its higher crustal abundance relative to tellurium (Te), silver's classification as a precious metal substantially elevates the production cost of MgAgSb, placing it above that of most conventional thermoelectric materials.

(2) Low-temperature TE performance. Although the room-temperature *ZT* of MgAgSb has been enhanced through multi-scale defect engineering and optimization of synthesis protocols, it remains notably inferior to that of p-type Bi_2Te_3. Consequently, the overall cooling performance of Mg-based devices continues to lag behind that of commercial Bi_2Te_3 counterparts, representing a significant barrier to their large-scale deployment. Hence, further elevating the *ZT* of MgAgSb at room and sub-ambient temperatures emerges as a critical imperative for future research.

(3) Device stability. In terms of the application of Mg-based power generation devices, ensuring long-term operational stability of the devices under real-world conditions warrants paramount attention. This encompasses not only the intrinsic stability of both p-type and n-type materials, but also the environmental resilience of TEiMs—particularly their oxidation resistance in air—and, most critically, the thermal and chemical stability of the solder joints.

In summary, the past decade has witnessed remarkable advancements in MgAgSb, encompassing optimization of the synthesis process, engineering of interface materials, and design and fabrication of devices. Nevertheless, substantial challenges persist, and concerted efforts remain imperative to surmount the barriers hindering its large-scale practical deployment.

Author contributions

Liangjun Xie: conceptualization, writing – original draft, writing – review & editing. Ran He: conceptualization, review, supervision, and funding acquisition. Jiehe Sui: review and supervision. Kornelius Nielsch: review and supervision. Zihang Liu: conceptualization, review and editing, supervision, and funding acquisition.

Conflicts of interest

There are no conflicts to declare.

Data availability

No primary research results, software or code have been included and no new data were generated or analysed as part of this review.

Acknowledgements

This work was funded by the National Natural Science Foundation of China (No. 22409043 and U23A20556) and European Union's Horizon European Research Council Programme (ERC Starting Grant, TENTATION, 101116340).

References

1 G. J. Snyder and E. S. Toberer, Complex Thermoelectric Materials, *Nat. Mater.*, 2008, 7, 105–114.
2 B. Jiang, Y. Yu, J. Cui, X. Liu, L. Xie, J. Liao, Q. Zhang, Y. Huang, S. Ning, B. Jia, B. Zhu, S. Bai, L. Chen,

S. J. Pennycook and J. He, High-Entropy-Stabilized Chalcogenides with High Thermoelectric Performance, *Science*, 2021, **371**, 830–834.

3 J. He and T. M. Tritt, Advances in thermoelectric materials research: Looking back and moving forward, *Science*, 2017, **357**, eaak9997.

4 X. L. Shi, N. H. Li, M. Li and Z. G. Chen, Toward Efficient Thermoelectric Materials and Devices: Advances, Challenges, and Opportunities, *Chem. Rev.*, 2025, **125**(16), 7525–7724.

5 K. Shen, Q. Yang, P. Qiu, Z. Zhou, S. Yang, T. R. Wei and X. Shi, Ductile P-Type AgCu(Se,S,Te) Thermoelectric Materials, *Adv. Mater.*, 2024, e2407424, DOI: 10.1002/adma.202407424.

6 S. Liu, Y. Qin, Y. Wen, H. Shi, B. Qin, T. Hong, X. Gao, Q. Cao, C. Chang and L. D. Zhao, Efforts Toward the Fabrication of Thermoelectric Cooling Module Based on N-Type and P-Type PbTe Ingots, *Adv. Funct. Mater.*, 2024, **34**, 2315707.

7 F. Jiang, C. Lin, J. Cheng, H. Yu, Y. Zhou, X. Ma, L. Wu, S. Ye, J. Chen, S. Zhi, Y. Xu, P. Zhao, X. Wang, F. Cao, Q. Zhang and J. Mao, Prefer-Oriented Ag_2Se Crystal for High-Performance Thermoelectric Cooling, *Adv. Funct. Mater.*, 2024, **35**, 2415000.

8 Y. Zhu, Y. Yu, H. Zhang, Y. Qin, Z.-Y. Wang, S. Zhan, D. Liu, N. Lin, Y. Tao, T. Hong, S. Wang, Z.-H. Ge, M. Wuttig and L.-D. Zhao, Large Mobility Enables Higher Thermoelectric Cooling and Power Generation Performance in n-type $AgPb_{18+x}SbTe_{20}$ Crystals, *J. Am. Chem. Soc.*, 2023, **145**, 24931–24939.

9 B. He, Y. He, W. Wang, Y. Sun, S. Kong, J. Huang, Y. Ru, B. Qin, H. Ren, J. He, T. Zhao, J. Li, J. Lu, L. D. Zhao and M. Liu, Strain-coupled, crystalline polymer-inorganic interfaces for efficient magnetoelectric sensing, *Science*, 2025, **389**, 623–631.

10 K. Zhao, Z. Yue, H. Wuliji, H. Chen, T. Deng, J. Lei, P. Qiu, L. Chen and X. Shi, Modeling critical thermoelectric transports driven by band broadening and phonon softening, *Nat. Commun.*, 2024, **15**, 776.

11 M. Papapetrou, G. Kosmadakis, A. Cipollina, U. La Commare and G. Micale, Industrial waste heat: Estimation of the technically available resource in the EU per industrial sector, temperature level and country, *Appl. Therm. Eng.*, 2018, **138**, 207–216.

12 Photographic Periodic Table, Abundance in Earth's Crust of the elements, https://periodictable.com/Properties/A/CrustAbundance.an.html.

13 X. Zhang, H. Zhu, X. Dong, Z. Fan, Y. Yao, N. Chen, J. Yang, K. Guo, J. Hao, L. He, G. Li and H. Zhao, High-performance $MgAgSb/Mg_3(Sb,Bi)_2$-based thermoelectrics with $\eta = 12\%$ at $T \leq 583$ K, *Joule*, 2024, **8**, 3324–3335.

14 X. Zhang, N. Chen, K. Guo, Q. Zhang, Q. Zhao, J. Xu, H. Zhu and H. Zhao, High cooling and power generation performance of α-MgAgSb with intrinsic low lattice thermal conductivity, *Mater. Today Phys.*, 2024, **44**, 101451.

15 L. Xie, G. Peng, Y. Sun, Z. Liu, F. Li, Y. Zhu, J. Zhu, H. Wu, N. Qu, W. Shi, L. Jiao, F. Guo, W. Cai, H. Wu and J. Sui, Semiconductor-Semimetal Composite Engineering Enabling Record-High Thermoelectric Power Density for Low-Temperature Energy Harvesting, *Adv. Funct. Mater.*, 2024, **34**, 2401763.

16 L. Xie, J. Yang, Z. Liu, N. Qu, X. Dong, J. Zhu, W. Shi, H. Wu, G. Peng, F. Guo, Y. Zhang, W. Cai, H. Wu, H. Zhu, H. Zhao, Z. Liu and J. Sui, Highly efficient thermoelectric cooling performance of ultrafine-grained and nanoporous materials, *Mater. Today*, 2023, **65**, 5–13.

17 J. Li, G. Li, Q. Chen, J. Feng, T. Feng, L. Xi, W. Liu, W. Zhang, R. Liu and R. Sun, Manipulating Anti-Site Defects in α-MgAgSb for Thermoelectric Cooling Enhancement, *Interdiscip. Mater.*, 2025, **4**(5), 719–727.

18 P. Ying, L. Wilkens, H. Reith, N. P. Rodriguez, X. Hong, Q. Lu, C. Hess, K. Nielsch and R. He, A Robust Thermoelectric Module Based on $MgAgSb/Mg_3(Sb, Bi)_2$ with a Conversion Efficiency of 8.5% and A Maximum Cooling of 72 K, *Energy Environ. Sci.*, 2022, **15**, 2557–2566.

19 Z. Liu, W. Gao, H. Oshima, K. Nagase, C.-H. Lee and T. Mori, Maximizing the Performance of N-type Mg_3Bi_2 Based Materials for Room-Temperature Power Generation and Thermoelectric Cooling, *Nat. Commun.*, 2022, **13**, 1120.

20 X. Dong, L. Jiao, H. Tong, H. Wu, H. Liang, X. Zhang, L. Wang, Q. Wen, M. Liu, Z. Ge, F. Guo, D. Luo, Y.-K. Zhu, Z. Liu, W. Cai and J. Sui, Heavy doping driven ultra-low lattice thermal conductivity and mechanical enhancement in $Mg_3(Bi, Sb)_2$ for efficient power generation, *Acta Mater.*, 2025, **300**, 121451.

21 G. Zhu, W. Liu, Y. Lan, G. Joshi, H. Wang, G. Chen and Z. Ren, The effect of secondary phase on thermoelectric properties of Zn_4Sb_3 compound, *Nano Energy*, 2013, **2**, 1172–1178.

22 M. Wang, Q. Zhang, K. Pang, M. Yuan, Q. Pan, R. Li, L. Miao, X. Tan, H. Hu, J. Wu, P. Sun, G. Q. Liu and J. Jiang, Robust Homogeneous Segmented Power Generator Driven by Sb_2Te_3-Based Thermoelectrics, *Adv. Mater.*, 2025, **37**, e2503128.

23 J. Du, Y. Sun, F. Guo, H. Tong, Z. Yu, Z. Liu, J. Zhu and J. Sui, Enhanced Thermoelectric Cooling Performance of $(Bi, Sb)_2Te_3$ Through Platinum Doping, *Mater. Today Phys.*, 2025, **53**, 101705.

24 J. Hu, Y. Sun, H. Wu, Z. Yu, J. Zhu, F. Guo, Z. Liu, W. Cai and J. Sui, All-Mg_3Sb_2-Based Module for Thermoelectric Power Generation, *Adv. Funct. Mater.*, 2024, **35**, 2418244.

25 R. H. Naderloo, R. B. Villoro, D. A. Mattlat, P. Ying, S. Song, S. Bayesteh, K. Nielsch, C. Scheu, Z. Ren, H. Zhu, S. Zhang and R. He, Performance advancements in P-type TaFeSb-based thermoelectric materials through composition and composite optimizations, *Energy Environ. Sci.*, 2025, **18**, 738–749.

26 P. Dharmaiah, M. Heo, C. Nagarjuna, S.-J. Jung, S. O. Won, K. H. Lee, S. K. Kim, J.-S. Kim, B. Ahn, H.-S. Kim and S.-H. Baek, Enhancement of thermoelectric properties in p-type ZnSb alloys through Cu-doping, *J. Alloys Compd.*, 2024, **1004**, 175739.

27 X. Ai, W. Xue, L. Giebeler, N. Pérez, B. Lei, Y. Zhang, Q. Zhang, K. Nielsch, Y. Wang and R. He, Interstitial

Defect Modulation Promotes Thermoelectric Properties of p-Type HfNiSn, *Adv. Energy Mater.*, 2024, **14**, 2401345.

28 H. Zhu, W. Li, A. Nozariasbmarz, N. Liu, Y. Zhang, S. Priya and B. Poudel, Half-Heusler alloys as emerging high power density thermoelectric cooling materials, *Nat. Commun.*, 2023, **14**, 3300.

29 G. K. Ren, S. Wang, Z. Zhou, X. Li, J. Yang, W. Zhang, Y. H. Lin, J. Yang and C. W. Nan, Complex electronic structure and compositing effect in high performance thermoelectric BiCuSeO, *Nat. Commun.*, 2019, **10**, 2814.

30 M. Li, S. M. K. N. Islam, M. Yahyaoglu, D. Pan, X. Shi, L. Chen, U. Aydemir and X. Wang, Ultrahigh figure-of-merit of Cu_2Se incorporated with carbon coated boron nanoparticles, *InfoMat*, 2019, **1**, 108–115.

31 M. Liu, M. Guo, H. Lyu, Y. Lai, Y. Zhu, F. Guo, Y. Yang, K. Yu, X. Dong, Z. Liu, W. Cai, M. Wuttig, Y. Yu and J. Sui, Doping strategy in metavalently bonded materials for advancing thermoelectric performance, *Nat. Commun.*, 2024, **15**, 8286.

32 H. Luo, X. L. Shi, Y. Liu, M. Li, M. Zhang, X. Luo, M. Wang, X. Huang, L. Hu and Z. G. Chen, Metavalent alloying and vacancy engineering enable state-of-the-art cubic GeSe thermoelectrics, *Nat. Commun.*, 2025, **16**, 3136.

33 H. Shi, Y. Wen, S. Bai, C. Chang, L. Su, T. Gao, S. Liu, D. Liu, B. Qin, Y. Qin, H. Liang, X. Qian, Z. Hou, X. Gao, T. Zhou, Q. Tan and L. D. Zhao, Crystal symmetry modification enables high-ranged in-plane thermoelectric performance in n-type SnSe crystals, *Nat. Commun.*, 2025, **16**, 1788.

34 T. Gao, Y. Wen, S. Bai, L. Su, H. Shi, R. Liu, S. Wang, Y. Hu, S. Liu, D. Liu, S. Liu, C. Liang, X. Feng, X. Wang, Y. Qin, X. Gao, B. Qin, C. Chang, P. Bai and L. D. Zhao, Extending the temperature range of the Cmcm phase of SnSe for high thermoelectric performance, *Science*, 2025, **390**, 1266–1271.

35 K. Pang, L. Miao, Q. Zhang, Q. Pan, Y. Liu, H. Shi, J. Li, W. Zhou, Z. Zhang, Y. Zhang, G. Wu, X. Tan, J. G. Noudem, J. Wu, P. Sun, H. Hu, G. Q. Liu and J. Jiang, Gradient Nanotwins and Enhanced Weighted Mobility Synergistically Upgrade $Bi_{0.5}Sb_{1.5}Te_3$ Thermoelectric and Mechanical Performance, *Adv. Funct. Mater.*, 2024, **34**, 2315591.

36 X. Hu, P. Jood, M. Ohta, M. Kunii, K. Nagase, H. Nishiate, M. G. Kanatzidis and A. Yamamoto, Power Generation from Nanostructured PbTe-based Thermoelectrics: Comprehensive Development from Materials to Modules, *Energy Environ. Sci.*, 2016, **9**, 517–529.

37 J. Cheng, L. Yin, X. Wang, S. Duan, P. Zhao, X. Ma, X. Li, X. Bao, S. Zhi, J. Mao, F. Cao and Q. Zhang, Realizing a Superior Conversion Efficiency of approximately 11.3% in the Group IV-VI Thermoelectric Module, *Small*, 2024, **20**, e2312145.

38 L. Xie, C. Ming, Q. Song, C. Wang, J. Liao, L. Wang, C. Zhu, F. Xu, Y. Y. Sun, S. Bai and L. Chen, Lead-free and scalable GeTe-based thermoelectric module with an efficiency of 12%, *Sci. Adv.*, 2023, **9**, eadg7919.

39 W. Shi, D. Qin, Y. Sun, H. Wu, H. Tong, L. Xie, Z. Liu, Q. Zhang, W. Cai, F. Guo and J. Sui, Batch Fabrication and Interface Stabilization Accelerate Application of Skutterudite Thermoelectric Module for Power Generation, *Adv. Energy Mater.*, 2024, **14**, 2303698.

40 J. Xia, J. Yang, Y. Wang, B. Jia, S. Li, K. Sun, Q. Zhao, D. Mao, H. F. Li and J. He, Synergistic Entropy Engineering with Vacancies: Unraveling the Cocktail Effect for Extraordinary Thermoelectric Performance in SnTe-Based Materials, *Adv. Funct. Mater.*, 2024, **34**, 2401635.

41 J. Hu, Y. Sun, W. Shi, H. Wu, J. Zhu, J. Cheng, L. Jiao, X. Jiang, L. Xie, N. Qu, F. Li, Z. Yu, Q. Zhang, Z. Liu, F. Guo, W. Cai and J. Sui, Realizing Ultrahigh Conversion Efficiency of approximately 9.0% in $YbCd_2Sb_2/Mg_3Sb_2$ Zintl Module for Thermoelectric Power Generation, *Adv. Mater.*, 2024, **36**, e2411738.

42 Q. Deng, F. Zhang, X. Yang, R. Li, C. Xia, P. Nan, Y. Chen, B. Ge, R. Ang and J. He, Ordered Grain Boundary Reconstruction Induces High-Efficiency Thermoelectric Power Generation in SnTe, *Energy Environ. Sci.*, 2024, **17**, 9467–9478.

43 S. Wan, Q. Song, H. Chen, Q. Zhang, J. Liao, X. Xia, C. Wang, P. Qiu, B. Chen, S. Bai and L. Chen, High-efficiency segmented thermoelectric power generation modules constructed from all skutterudites, *Cell Rep. Phys. Sci.*, 2023, **4**, 101651.

44 X. Wu, Y. Lin, Z. Han, H. Li, C. Liu, Y. Wang, P. Zhang, K. Zhu, F. Jiang, J. Huang, H. Fan, F. Cheng, B. Ge and W. Liu, Interface and Surface Engineering Realized High Efficiency of 13% and Improved Thermal Stability in $Mg_3Sb_{1.5}Bi_{0.5}$-Based Thermoelectric Generation Devices, *Adv. Energy Mater.*, 2022, **12**, 2203039.

45 R. Liu, Y. Xing, J. Liao, X. Xia, C. Wang, C. Zhu, F. Xu, Z. G. Chen, L. Chen, J. Huang and S. Bai, Thermal-inert and ohmic-contact interface for high performance half-Heusler based thermoelectric generator, *Nat. Commun.*, 2022, **13**, 7738.

46 Y. Fu, Q. Zhang, Z. Hu, M. Jiang, A. Huang, X. Ai, S. Wan, H. Reith, L. Wang, K. Nielsch and W. Jiang, $Mg_3(Bi, Sb)_2$-based Thermoelectric Modules for Efficient and Reliable Waste-Heat Utilization up to 750 K, *Energy Environ. Sci.*, 2022, **15**, 3265–3274.

47 D. Liu, D. Wang, T. Hong, Z. Wang, Y. Wang, Y. Qin, L. Su, T. Yang, X. Gao, Z. Ge, B. Qin and L.-D. Zhao, Lattice Plainification Advances Highly Effective SnSe Crystalline Thermoelectrics, *Science*, 2023, **380**, 841–846.

48 Z. Zhang, R. Ji, M. Kroll, Y. J. Hofstetter, X. Jia, D. Becker-Koch, F. Paulus, M. Löffler, F. Nehm, K. Leo and Y. Vaynzof, Efficient Thermally Evaporated γ-$CsPbI_3$ Perovskite Solar Cells, *Adv. Energy Mater.*, 2021, **11**(29), 2100299.

49 R. Ji, Z. Zhang, M. Deconinck, Y. J. Hofstetter, J. Shi, F. Paulus, P. Raval, G. N. M. Reddy and Y. Vaynzof, Spontaneous Formation of 1D/3D Perovskite Heterojunctions for Efficient Inverted Perovskite Solar Cells, *Adv. Energy Mater.*, 2024, **14**(12), 2304126.

50 T. Zhu, Y. Liu, C. Fu, J. P. Heremans, J. G. Snyder and X. Zhao, Compromise and Synergy in High-Efficiency

Thermoelectric Materials, *Adv. Mater.*, 2017, **29**(14), 1605884.

51 G. J. Snyder and A. H. Snyder, Figure of merit ZT of a thermoelectric device defined from materials properties, *Energy Environ. Sci.*, 2017, **10**, 2280–2283.

52 Y. Liao, J.-L. Chen, C. Liu, J. Liang, Q. Zhou, P. Wang and L. Miao, Sintering Pressure as a "Scalpel" to Enhance the Ehermoelectric Performance of MgAgSb, *J. Mater. Chem. C*, 2022, **10**, 3360–3367.

53 K. Guo, X. Zhang, Z. Fan, Y. Wang, J. Yang, H. Zhu, J. Chen, Q. Zhao, Z. Li, S. Wang, Q. Zhang, Y. Yao, L. He and H. Zhao, Rational manipulation of Ag vacancies for lattice plainification and superior thermoelectric performance in α-MgAgSb, *Chem. Eng. J.*, 2025, **507**, 160515.

54 J. Xin, J. Yang, S. Li, A. Basit, B. Sun, S. Li, Q. Long, X. Li, Y. Chen and Q. Jiang, Thermoelectric Performance of Rapidly Microwave-Synthesized α-MgAgSb with SnTe Nanoinclusions, *Chem. Mater.*, 2019, **31**, 2421–2430.

55 A. Duparchy, L. Millerand, J. Camut, S. Tumminello, H. Kamila, R. Deshpande, A. Cowley, E. Mueller and J. de Boor, Establishing Synthesis-Composition-Property Relationships for Enhanced and Reproducible Thermoelectric Properties of MgAgSb, *J. Mater. Chem. A*, 2022, **10**, 21716–21726.

56 I. Rodriguez-Barber, J. Camut, L. Luhmann, A. Cowley, E. Mueller and J. de Boor, On the influence of AgMg precursor formation on MgAgSb microstructure and thermoelectric properties, *J. Alloys Compd.*, 2021, **860**, 158384.

57 J. Camut, I. Barber Rodriguez, H. Kamila, A. Cowley, R. Sottong, E. Mueller and J. de Boor, Insight on the Interplay between Synthesis Conditions and Thermoelectric Properties of α-MgAgSb, *Materials*, 2019, **12**, 1857.

58 S. Y. Back, S. Meikle and T. Mori, Comprehensive study of α-MgAgSb: Microstructure, carrier transport properties, and thermoelectric performance under ball milling techniques, *J. Mater. Sci. Technol.*, 2025, **227**, 57–66.

59 F. Qiu, J.-L. Chen, Y. Liao, Z. Zhang, J. Liang, L. Miao, Q. Zhou, Y. Peng, C. Liu and J. Gao, Realization of high cryogenic thermoelectric performance for MgAgSb base alloy by regulation heat-treatment process, *Appl. Phys. Lett.*, 2024, **124**, 173902.

60 Z. Liu, J. Mao, J. Sui and Z. Ren, High thermoelectric performance of α-MgAgSb for power generation, *Energy Environ. Sci.*, 2018, **11**, 23–44.

61 A. A. Ivanov, E. P. Kaplar, Y. P. Prilepo, V. V. Murav'ev and V. S. Ustinov, Progress in the Research on Promising High-Performance Thermoelectric Materials, *Nanobiotechnol. Rep.*, 2021, **16**, 268–281.

62 Y. Iqbal, J. Wang, C. Wang, P. Muhammad, A. Zada, M. Khan, H. Maab, Q. Khan and M. Maqbool, ThermoelectricMgAgSballoys for sustainable energy application, *Int. J. Energy Res.*, 2022, **46**, 22266–22284.

63 L. Wang, L. Yin, J. Mao, Q. Zhang, J. Sui and Z. Liu, Half-Heusler compounds and devices for mid-high temperature thermoelectric applications, *MRS Bull.*, 2025, **50**, 945–955.

64 W. Zuo, H. Chen, Z. Yu, Y. Fu, X. Ai, Y. Cheng, M. Jiang, S. Wan, Z. Fu, R. Liu, G. Cheng, R. Xu, L. Wang, F. Xu, Q. Zhang, D. Makarov and W. Jiang, Atomic-scale interface strengthening unlocks efficient and durable Mg-based thermoelectric devices, *Nat. Mater.*, 2025, **24**, 735–742.

65 A. Li, L. Wang, J. Li, X. Wu and T. Mori, Self-optimized contact in air-robust thermoelectric junction towards long-lasting heat harvesting, *Nat. Commun.*, 2025, **16**, 1502.

66 S. Chen, T. Zhang, J. Cheng, B. Ma, X. Ma, X. Li, L. Yin, L. Wen, J. Mao, F. Cao and Q. Zhang, Unified contact layer and low-temperature transient liquid phase interconnection for high-performance all-Mg-based thermoelectric devices, *Natl. Sci. Rev.*, 2025, **12**, nwaf227.

67 X. Wu, Y. Lin, C. Liu, Y. Wang, H. Li, B. Ge and W. Liu, A high performance eco-friendly MgAgSb-based thermoelectric power generation device near phase transition temperatures, *Energy Environ. Sci.*, 2024, **17**, 2879–2887.

68 L. Xie, L. Yin, Y. Yu, G. Peng, S. Song, P. Ying, S. Cai, Y. Sun, W. Shi, H. Wu, N. Qu, F. Guo, W. Cai, H. Wu, Q. Zhang, K. Nielsch, Z. Ren, Z. Liu and J. Sui, Screening strategy for developing thermoelectric interface materials, *Science*, 2023, **382**, 921–928.

69 D. Kraemer, J. Sui, K. McEnaney, H. Zhao, Q. Jie, Z. F. Ren and G. Chen, High Thermoelectric Conversion Efficiency of MgAgSb-Based Material with Hot-Pressed Contacts, *Energy Environ. Sci.*, 2015, **8**, 1299–1308.

70 P. Ying, R. B. Villoro, A. Bahrami, L. Wilkens, H. Reith, D. A. Mattlat, V. Pacheco, C. Scheu, S. Zhang, K. Nielsch and R. He, Performance Degradation and Protective Effects of Atomic Layer Deposition for Mg-based Thermoelectric Modules, *Adv. Funct. Mater.*, 2024, **34**, 2406473.

71 H. Nowotny and W. Sibert, Ternäre Valenzverbindungen in den Systemen Kupfer(Silber)-Arsen(Antimon, Wismut)-Magnesium, *Int. J. Mater. Res.*, 1941, **33**, 391–394.

72 J.-L. Mi, P.-J. Ying, M. Sist, H. Reardon, P. Zhang, T.-J. Zhu, X.-B. Zhao and B. B. Iversen, Elaborating the Crystal Structures of MgAgSb Thermoelectric Compound: Polymorphs and Atomic Disorders, *Chem. Mater.*, 2017, **29**, 6378–6388.

73 M. J. Kirkham, A. M. dos Santos, C. J. Rawn, E. Lara-Curzio, J. W. Sharp and A. J. Thompson, Ab Initio Determination of Crystal Structures of the Thermoelectric Material MgAgSb, *Phys. Rev. B: Condens. Matter Mater. Phys.*, 2012, **85**, 144120.

74 Y. Huang, J. Lei, H. Chen, Z. Zhou, H. Dong, S. Yang, H. Gao, T.-R. Wei, K. Zhao and X. Shi, Intrinsically high thermoelectric performance in near-room-temperature α-MgAgSb materials, *Acta Mater.*, 2023, **249**, 118847.

75 P. Ying, X. Liu, C. Fu, X. Yue, H. Xie, X. Zhao, W. Zhang and T. Zhu, High Performance α-MgAgSb Thermoelectric Materials for Low Temperature Power Generation, *Chem. Mater.*, 2015, **27**, 909–913.

76 Z. Liu, Y. Wang, J. Mao, H. Geng, J. Shuai, Y. Wang, R. He, W. Cai, J. Sui and Z. Ren, Lithium Doping to Enhance

Thermoelectric Performance of MgAgSb with Weak Electron-Phonon Coupling, *Adv. Energy Mater.*, 2016, **6**, 1502269.

77 P. Ying, X. Li, Y. Wang, J. Yang, C. Fu, W. Zhang, X. Zhao and T. Zhu, Hierarchical Chemical Bonds Contributing to the Intrinsically Low Thermal Conductivity in α-MgAgSb Thermoelectric Materials, *Adv. Funct. Mater.*, 2017, **27**, 1604145.

78 Z. Liu, Y. Zhang, J. Mao, W. Gao, Y. Wang, J. Shuai, W. Cai, J. Sui and Z. Ren, The Microscopic Origin of Low Thermal Conductivity for Enhanced Thermoelectric Performance of Yb Doped MgAgSb, *Acta Mater.*, 2017, **128**, 227–234.

79 X. Li, P. F. Liu, E. Zhao, Z. Zhang, T. Guidi, M. D. Le, M. Avdeev, K. Ikeda, T. Otomo, M. Kofu, K. Nakajima, J. Chen, L. He, Y. Ren, X. L. Wang, B. T. Wang, Z. Ren, H. Zhao and F. Wang, Ultralow thermal conductivity from transverse acoustic phonon suppression in distorted crystalline alpha-MgAgSb, *Nat. Commun.*, 2020, **11**, 942.

80 H. Zhao, J. Sui, Z. Tang, Y. Lan, Q. Jie, D. Kraemer, K. McEnaney, A. Guloy, G. Chen and Z. Ren, High Thermoelectric Performance of MgAgSb-Based Materials, *Nano Energy*, 2014, **7**, 97–103.

81 J. Shuai, H. S. Kim, Y. Lan, S. Chen, Y. Liu, H. Zhao, J. Sui and Z. Ren, Study on Thermoelectric Performance by Na Doping in Nanostructured $Mg_{1-x}Na_xAg_{0.97}Sb_{0.99}$, *Nano Energy*, 2015, **11**, 640–646.

82 J. Sui, J. Shuai, Y. Lan, Y. Liu, R. He, D. Wang, Q. Jie and Z. Ren, Effect of Cu Concentration on Thermoelectric Properties of Nanostructured p-type $MgAg_{0.97-x}Cu_xSb_{0.99}$, *Acta Mater.*, 2015, **87**, 266–272.

83 Z. Liu, H. Geng, J. Mao, J. Shuai, R. He, C. Wang, W. Cai, J. Sui and Z. Ren, Understanding and manipulating the intrinsic point defect in α-MgAgSb for higher thermoelectric performance, *J. Mater. Chem. A*, 2016, **4**, 16834–16840.

84 Z. Liu, J. Shuai, J. Mao, Y. Wang, Z. Wang, W. Cai, J. Sui and Z. Ren, Effects of Antimony Content in $MgAg_{0.97}Sb_x$ on Output Power and Energy Conversion Efficiency, *Acta Mater.*, 2016, **102**, 17–23.

85 Z. Liu, W. Gao, X. Meng, X. Li, J. Mao, Y. Wang, J. Shuai, W. Cai, Z. Ren and J. Sui, Mechanical properties of nanostructured thermoelectric materials α-MgAgSb, *Scr. Mater.*, 2017, **127**, 72–75.

86 Z. Liu, Y. Wang, W. Gao, J. Mao, H. Geng, J. Shuai, W. Cai, J. Sui and Z. Ren, The Influence of Doping Sites on Achieving Higher Thermoelectric Performance for Nanostructured α-MgAgSb, *Nano Energy*, 2017, **31**, 194–200.

87 Y. Liu, D. Z. Zhou, Y. Q. Li, A. J. Hong, J. H. Sui, J. M. Liu and Z. F. Ren, Unusual consequences of donor and acceptor doping on the thermoelectric properties of the $MgAg_{0.97}Sb_{0.99}$ alloy, *J. Mater. Chem. A*, 2018, **6**, 2600–2611.

88 A. Li, L. Wang, J. Li and T. Mori, Global softening to manipulate sound velocity for reliable high-performance MgAgSb thermoelectrics, *Energy Environ. Sci.*, 2024, **17**(22), 8810–8819.

89 Z. Feng, J. Zhang, Y. Yan, G. Zhang, C. Wang, C. Peng, F. Ren, Y. Wang and Z. Cheng, Ag-Mg antisite defect induced high thermoelectric performance of alpha-MgAgSb, *Sci. Rep.*, 2017, **7**, 2572.

90 Z. Pang, X. Zhang and C. Wang, Investigation on native defects of α -MgAgSb and its effects on thermoelectric properties using first principles calculations, *Curr. Appl. Phys.*, 2017, **17**, 1279–1287.

91 L. Jiao, L. Xie, Y.-K. Zhu, L. Wang, Y. Sun, Y. Yu, A. Ivanova, V. Khovaylo, F. Guo, W. Cai, J. Sui and Z. Liu, Grain boundary segregation mediated highly stable and high performance nanostructured MgAgSb bulk thermoelectric materials, *Trans. Mater. Res.*, 2025, **1**, 100016.

92 Z. Bu, X. Zhang, Y. Hu, Z. Chen, S. Lin, W. Li, C. Xiao and Y. Pei, A Record Thermoelectric Efficiency in Tellurium-Free Modules for Low-Grade Waste Heat Recovery, *Nat. Commun.*, 2022, **13**, 237.

93 R. Bjørk, The Universal Influence of Contact Resistance on the Efficiency of a Thermoelectric Generator, *J. Electron. Mater.*, 2015, **44**, 2869–2876.

94 Y. Li, Y. Shi, D. Luo, X. Wang and Y. Yan, Impacts of distributed thermal and electric contact resistance on performance and geometric optimization of thermoelectric generators, *Appl. Therm. Eng.*, 2024, **246**, 122873.

95 Y. Rao, C. Xu, M. Voss, P. Ying, H. Reith, K. Nielsch, T. Bechtold and D. Hohlfeld, Fabrication and Characterization of a Thermoelectric Generator with High Aspect Ratio Thermolegs for Electrically Active Implants, *Adv. Mater. Technol.*, 2023, **9**, 2301157.

96 T. Xing, Q. Song, P. Qiu, Q. Zhang, M. Gu, X. Xia, J. Liao, X. Shi and L. Chen, High efficiency GeTe-based materials and modules for thermoelectric power generation, *Energy Environ. Sci.*, 2021, **14**, 995–1003.

97 J. Chu, M. Gu, R. Liu, S. Bai, X. Shi and L. Chen, Interfacial behaviors of p-type $Ce_yFe_xCo_{4-x}Sb_{12}$/Nb thermoelectric joints, *Funct. Mater. Lett.*, 2020, **13**, 2051020.

98 M. Gu, X. Xia, X. Li, X. Huang and L. Chen, Microstructural evolution of the interfacial layer in the Ti–Al/$Yb_{0.6}Co_4Sb_{12}$ thermoelectric joints at high temperature, *J. Alloys Compd.*, 2014, **610**, 665–670.

99 D. Zhao, X. Li, L. He, W. Jiang and L. Chen, Interfacial evolution behavior and reliability evaluation of $CoSb_3$/Ti/Mo–Cu thermoelectric joints during accelerated thermal aging, *J. Alloys Compd.*, 2009, **477**, 425–431.

100 L. Yin, X. Li, X. Bao, J. Cheng, C. Chen, Z. Zhang, X. Liu, F. Cao, J. Mao and Q. Zhang, CALPHAD accelerated design of advanced full-Zintl thermoelectric device, *Nat. Commun.*, 2024, **15**, 1468.

101 F. Li, S. Li, H. Wu, Y.-K. Zhu, W. Shi, X. Bao, Y. Jin, L. Wang, X. Dong, F. Guo, W. Cai, J. Zhu, Z. Liu and J. Sui, Phase penetration: key drivers in barrier layer failure of Hf-free Half-Heusler thermoelectric modules, *Sci. China Mater.*, 2025, 1–8.

102 P. Ying, R. He, J. Mao, Q. Zhang, H. Reith, J. Sui, Z. Ren, K. Nielsch and G. Schierning, Towards Tellurium-free Thermoelectric Modules for Power Generation from Low-grade Heat, *Nat. Commun.*, 2021, **12**, 1121.

103 Z. Liu, N. Sato, W. Gao, K. Yubuta, N. Kawamoto, M. Mitome, K. Kurashima, Y. Owada, K. Nagase, C.-H. Lee, J. Yi, K. Tsuchiya and T. Mori, Demonstration of Ultrahigh Thermoelectric Efficiency of ~7.3% in Mg_3Sb_2/MgAgSb Module for Low-Temperature Energy Harvesting, *Joule*, 2021, **5**, 1196–1208.

104 M. Gu, S. Bai, J. Wu, J. Liao, X. Xia, R. Liu and L. Chen, A high-throughput strategy to screen interfacial diffusion barrier materials for thermoelectric modules, *J. Mater. Res.*, 2019, **34**, 1179–1187.

105 R. Chetty, J. Babu and T. Mori, Improving Thermoelectric Conversion Efficiency of $Mg_3(Sb, Bi)_2$-Based TE Materials via Interface Contact Layer Optimization, *ACS Appl. Energy Mater.*, 2024, **7**, 12112–12118.

106 J. Yang, G. Li, H. Zhu, N. Chen, T. Lu, J. Gao, L. Guo, J. Xiang, P. Sun, Y. Yao, R. Yang and H. Zhao, Next-Generation Thermoelectric Cooling Modules Based on High-Performance $Mg_3(Bi, Sb)_2$ Material, *Joule*, 2022, **6**, 193–204.

107 P. Ying, H. Reith, K. Nielsch and R. He, Geometrical Optimization and Thermal-Stability Characterization of Te-Free Thermoelectric Modules Based on MgAgSb/$Mg_3(Bi, Sb)_2$, *Small*, 2022, **18**, e2201183.

108 L. Xie, H. Tong, G. Peng, H. Wu, W. Shi, K. Yu, J. Hu, L. Jiao, X. Dong, F. Guo, W. Cai, Y. Zhang, H. Wu, Z. Liu and J. Sui, Boosting carrier mobility in MgAgSb via in-situ InSb nanoprecipitates for high-efficiency segmented thermoelectric module, *Nat. Commun.*, 2025, **16**, 7484.

109 J.-L. Chen, Y. Liao, Q. Zhou, J. Liang, L. Miao, Y. Zhu, S. Wang, W. He, H. Nishiate, C.-H. Lee, M. Murata, H. Lai and Z. Li, Realizing high conversion efficiency in shallow cryogenic thermoelectric module based on n-type BiSb and p-type MgAgSb materials, *Mater. Today Phys.*, 2022, **28**, 100855.

110 A. Wieder, J. Camut, A. Duparchy, R. Deshpande, A. Cowley, E. Müller and J. de Boor, High-performance tellurium-free thermoelectric module for moderate temperatures using α-MgAgSb/Mg_2(Si, Sn), *Mater. Today Energy*, 2023, **38**, 101420.

111 S. Patra, P. Patro, P. Gupta, S. Singh and A. Singh, Harvesting low grade waste heat through environment friendly n-Ag_2Se/p-MgAgSb based thermoelectric module, *Emergent Mater.*, 2025, **8**(5), 3741–3752.

112 G. Tian, W. Shi, R. Guo, R. Guo, W. Zhang, D. Liu and C. Xue, Facile Y-type Micro Ag_2Se/MgAgSb flexible thermoelectric device based on lift-off technology, *Sci. Rep.*, 2024, **14**, 28247.

113 C. E. Whiting and D. F. Woerner, The Graph Becomes the Dataset: Compiling Historical and Current RTG Data into One Place, *Nucl. Technol.*, 2024, 1–8.

114 Z. Zhang, C. Ming, Q. Song, L. Wang, H. Chen, J. Liao, C. Wang, L. Chen and S. Bai, Grain boundary modulation improved thermal stability of high thermoelectric performance Mg3(Sb,Bi)2-based compounds, *Acta Mater.*, 2025, **287**, 120806.

115 Y. Geng, Z. Li, Z. Lin, Y. Liu, Q. Lai, X. Wu, L. Hu, F. Liu, Y. Yu and C. Zhang, Inhibiting Mg Diffusion and Evaporation by Forming Mg-Rich Reservoir at Grain Boundaries Improves the Thermal Stability of N-Type Mg_3Sb_2 Thermoelectrics, *Small*, 2024, **20**, e2305670.

116 X. Wu, X. Ma, H. Yao, K. Liang, P. Zhao, S. Hou, L. Yin, H. Yang, J. Sui, X. Lin, F. Cao, Q. Zhang and J. Mao, Revealing the Chemical Instability of $Mg_3Sb_{2-x}Bi_x$-Based Thermoelectric Materials, *ACS Appl. Mater. Interfaces*, 2023, **15**, 50216–50224.